MAGNETIC RESONANCE
Open Access Discussions

Improved NMR transfer of magnetization from protons to half-integer spin quadrupolar nuclei at moderate and high MAS frequencies

Jennifer S. Gómez[1], Andrew G.M. Rankin[1,#], Julien Trébosc[2], Frédérique Pourpoint [1], Yu Tsutsumi[3], Hiroki Nagashima[4], Olivier Lafon[1,5], Jean-Paul Amoureux[1,6,7]

[1]Univ. Lille, CNRS, Centrale Lille, Univ. Artois, UMR 8181 – UCCS – Unité de Catalyse et Chimie du Solide, Lille, 59000, France
[2]Univ. Lille, CNRS, INRAE, Centrale Lille, Univ. Artois, FR 2638 – IMEC – Fédération Chevreul, Lille, 59000, France
[3]Bruker Japan, 3-9 Moriya-cho, Kanagawa-ku, Yokohama-shi, Kanagawa, 221-0022, Japan
[4]Interdisciplinary Research Center for Catalytic Chemistry, National Institute of Advanced Industrial Science and Technology (AIST), 1-1-1 Higashi, Tsukuba, Ibaraki, 305-8565, Japan
[5]Institut Universitaire de France, 1 rue Descartes, Paris, 75231, France
[6]Riken NMR Science and Development Division, Yokohama-shi, Yokohama-shi, Kanagawa, 230-0045, Japan
[7]Bruker Biospin, 34 rue de l'industrie, Wissembourg, 67166, France
[#]Present address: Sorbonne Université, CNRS, Collège de France, Laboratoire de Chimie de la Matière Condensée de Paris (LCMCP), 4 place Jussieu, Paris, 75005, France

Correspondance to: Olivier Lafon (olivier.lafon@univ-lille.fr) and Jean-Paul Amoureux (jean-paul.amoureux@univ-lille.fr)

Abstract. Half-integer spin quadrupolar nuclei are the only magnetic isotopes for the majority of the chemical elements. Therefore, the transfer of polarization from protons to these isotopes under magic-angle spinning (MAS) can provide precious insights into the interatomic proximities in hydrogen-containing solids, including organic, hybrid, nanostructured and biological solids. Furthermore, this transfer has recently been combined with dynamic nuclear polarization (DNP) in order to enhance the NMR signal of half-integer quadrupolar isotope. Nevertheless, the cross-polarization transfer lacks of robustness in the case of quadrupolar nuclei and we have recently introduced as an alternative technique a through-space refocused insensitive nuclei enhancement by polarization transfer (*D*-RINEPT) scheme combining hetero-nuclear dipolar recoupling built from adiabatic pulses and continuous wave decoupling. This technique has been demonstrated at 9.4 T with moderate MAS frequencies, $\nu_R \approx$ 10-15 kHz, in order to transfer the DNP-enhanced ^{1}H polarization to quadrupolar nuclei. Nevertheless, polarization transfers from protons to quadrupolar nuclei are also required at higher MAS frequencies in order to improve the resolution of ^{1}H spectra. We investigate how this transfer can be achieved at $\nu_R \approx$ 20 and 60 kHz. We demonstrate that the *D*-RINEPT sequence using adiabatic pulses still produces efficient and robust transfer but requires large rf-fields, which may not be compatible with the specifications of commonly employed MAS NMR probes. As an alternative, we introduce robust and efficient variants of *D*-RINEPT and PRESTO (phase-shifted recoupling effects a smooth transfer of order) sequences using symmetry-based recoupling schemes built from single and composite π-pulses. Their performances are compared using the

MAGNETIC
RESONANCE
Discussions

35   average Hamiltonians and experiments at $B_0 = 18.8$ T on γ-alumina and isopropylamine templated microporous aluminophosphate $AlPO_4$-14, featuring low and significant ^1H-^1H dipolar interactions, respectively. These experiments demonstrate that the ^1H magnetization can be efficiently transferred to ^{27}Al nuclei using D-RINEPT with $SR4_1^2(270_090_{180})$ recoupling, and PRESTO with $R22_2^7(180_0)$ or $R16_7^6(270_090_{180})$ schemes at $\nu_R = 20$ or 62.5 kHz, respectively. The D-RINEPT and PRESTO recouplings complement each other since the latter is affected by dipolar truncation, whereas the former is not.

40

I. Introduction

Quadrupolar nuclei with a nuclear spin quantum number $S = 3/2, 5/2, 7/2$ or $9/2$ are the only NMR-active isotopes for over 60% of the chemical elements of the first six periods of the periodic table, including six of the eight most abundant elements by mass in the Earth's crust: O, Al, Ca, Na, Mg and K.(Ashbrook and Sneddon, 2014) A wide range of materials, including

45   organic compounds, biological macromolecules as well as nanostructured or hybrid materials, contain half-integer spin quadrupolar nuclei and protons. Proximities between these isotopes have notably been probed in solid-state NMR experiments by transferring the polarization of protons to half-integer quadrupolar nuclei through dipolar couplings under magic-angle spinning (MAS) conditions.(Rocha et al., 1991; Hwang et al., 2004; Peng et al., 2007; Vogt et al., 2013; Chen et al., 2019) More recently, this polarization transfer has been combined under MAS with DNP (dynamic nuclear polarization) in order to

50   enhance the NMR signals of half-integer spin quadrupolar nuclei.(Vitzthum et al., 2012; Perras et al., 2015a; Nagashima et al., 2020) This approach has notably allowed the detection of insensitive quadrupolar nuclei with low natural abundance, such as ^{17}O or ^{43}Ca, or low gyromagnetic ratio, γ, such as $^{47,49}Ti$, ^{67}Zn or ^{95}Mo, near surfaces of materials.(Perras et al., 2015a; Nagashima et al., 2020; Blanc et al., 2013; Perras et al., 2016, 2017; Hope et al., 2017; Lee et al., 2017; Nagashima et al., n.d.; Li et al., 2018)

55   This transfer has originally been achieved using cross-polarization under MAS (CPMAS).(Harris and Nesbitt, 1988) Nevertheless, this technique lacks robustness for quadrupolar nuclei since the spin-locking of the central transition (CT) between energy levels ±1/2 is sensitive to the strength of the quadrupole interaction, the offset, the CSA (chemical shift anisotropy) and the rf-field inhomogeneity.(Vega, 1992; Amoureux and Pruski, 2002; Tricot et al., 2011, p.20) Furthermore, CPMAS experiments require a careful adjustment of the rf-field applied to the quadrupolar isotope in order to fulfill the

60   Hartmann-Hahn condition $(S+1/2)\nu_{1S} + \varepsilon\nu_{1H} = n\nu_R$, where ν_{1S} and ν_{1H} denote the amplitudes of the rf-fields applied to the quadrupolar isotope S and to the protons, respectively, $\varepsilon = \pm1$, $n = \pm1$ or ±2, and ν_R is the MAS speed, while avoiding the rotary resonance recoupling (R^3) $\nu_{1S} = p\nu_R/(S+1/2)$ with $p = 0, 1, 2, 3$.(Amoureux and Pruski, 2002; Ashbrook and Wimperis, 2009) Moreover, the magnetization of the quadrupolar nuclei cannot be spin-locked for some crystallite orientations, which leads to line-shape distortions.(Barrie, 1993; Hayashi and Hayamizu, 1993; Ding and Mcdowell, 1995)

65   These issues have been circumvented by the use of the PRESTO (phase-shifted recoupling effects a smooth transfer of order) scheme,(Perras et al., 2015a, b) and more recently, the through-space refocused INEPT (denoted RINEPT

hereafter).(Nagashima et al., 2020, n.d.; Giovine et al., 2019) These schemes benefit from higher robustness than CPMAS since they do not employ a spin-lock on the quadrupolar channel, but instead a limited number (two or three) of pulses selective to the CT. In these sequences, the dipolar interactions between protons and quadrupolar nucleus are reintroduced by applying

70   on the ^{1}H channel symmetry-based recoupling sequences, such as $R18_2^5$ for PRESTO or $SR4_1^2$ for RINEPT.(Zhao et al., 2001; Brinkmann and Kentgens, 2006a) In the case of recoupling sequences built from single square π-pulses, the RINEPT sequence using $SR4_1^2$ (denoted RINEPT-$SR4_1^2$) is more efficient than PRESTO at $\nu_R \geq 60$ kHz because of its higher robustness to rf-field inhomogeneity and ^{1}H offset and CSA. At $\nu_R \leq 20$ kHz, the PRESTO technique is more efficient since the efficiency of RINEPT-$SR4_1^2$ is reduced by the increased losses due to ^{1}H-^{1}H interactions at lower MAS frequencies during the $SR4_1^2$

75   recoupling and the windows used to rotor-synchronize the $SR4_1^2$ blocks, whereas the PRESTO sequence is devoid of these windows.(Giovine et al., 2019a)

Recently, we have introduced a novel variant of the RINEPT sequence employing $SR4_1^2$ recoupling built (i) from tanh/tan (tt) adiabatic inversion pulses, (ii) continuous-wave (CW) irradiations during the windows, and (iii) composite $\pi/2$ and π pulses on the ^{1}H channel, in order to limit the losses due to ^{1}H-^{1}H interactions and improve the transfer efficiency at moderate MAS

80   frequencies.(Nagashima et al., 2020, n.d.) This novel RINEPT variant, denoted RINEPT-CWc-$SR4_1^2$(tt), is more efficient than PRESTO and CPMAS at $\nu_R \approx 12.5$ kHz and has been combined with DNP to detect the NMR signal of quadrupolar nuclei with small dipolar coupling with protons, including quadrupolar low-γ isotopes, such as ^{47,49}Ti, ^{67}Zn or ^{95}Mo, and unprotonated ^{17}O nuclei.

However, several NMR experiments require the transfer of ^{1}H magnetization to quadrupolar nuclei at $\nu_R > 12.5$ kHz. In

85   particular, MAS frequencies of $\nu_R \geq 20$ kHz are needed to avoid the overlap between the center-bands and the spinning sidebands of satellite transitions (ST) in ^{27}Al spectra at 18.8 T. In addition, magnetization transfers at $\nu_R \geq 60$ kHz are advantageous to acquire 2D hetero-nuclear correlation spectra between protons and quadrupolar nuclei endowed with high resolution along the ^{1}H dimension since fast MAS averages out the ^{1}H-^{1}H dipolar couplings.

Concurrently, we have demonstrated that the efficiency of PRESTO transfers using the $R16_7^6$ recoupling can be improved at

90    $\nu_R = 62.5$ kHz using $270_0 90_{180}$ composite π-pulses as a basic inversion element, where the standard notation for composite pulses is used: ξ_ϕ denotes a rectangular, resonant rf-pulse with flip angle ξ and phase ϕ in degrees.(Giovine et al., 2019a) More recently, $SR4_1^2$ and $R12_3^5$ recoupling schemes built from $90_{-45} 90_{45} 90_{-45}$ composite π-pulses have been proposed, but they have not yet been incorporated into RINEPT transfers.(Perras et al., 2019) Globally, no systematic study of RN_n^ν recouplings built from composite π-pulses has been carried out.

95   In the present article, we investigate the use of RINEPT-CWc using an adiabatic recoupling scheme at the higher MAS frequencies of $\nu_R = 20$ and 62.5 kHz. We demonstrate using numerical simulations of spin dynamics and experiments on γ-alumina and isopropylamine templated microporous aluminophosphate AlPO$_4$-14 (hereafter AlPO$_4$-14) that the rf requirement of this technique increases with the ^{1}H-^{1}H dipolar interactions and is not compatible with the specifications of most MAS probes at $\nu_R \geq 20$ kHz. As an alternative, we introduce variants of the PRESTO and RINEPT sequences by selecting with AH

MAGNETIC RESONANCE
Discussions

100 (average Hamiltonian) the recoupling schemes built from single rectangular or composite π-pulses. Finally, using experiments on γ-alumina and $AlPO_4$-14, which feature different ^{1}H-^{1}H dipolar interactions, we identify the most robust and efficient PRESTO and RINEPT transfers at $B_0 = 18.8$ T with $\nu_R = 20$ and 62.5 kHz.
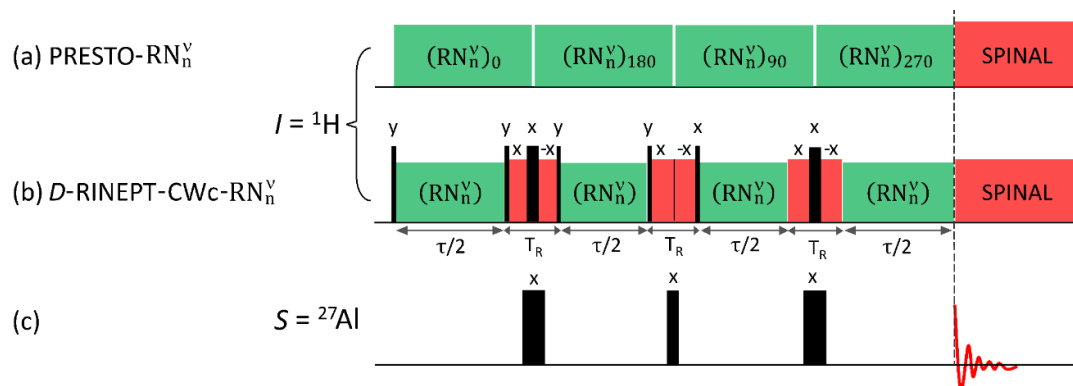
105 Figure 1: ^{1}H $\rightarrow$ ^{27}Al (a,c) PRESTO-RN$_n^\nu$ and (b,c) *D*-RINEPT-CWc-RN$_n^\nu$ pulse sequences. The sequences applied to ^{1}H and ^{27}Al channels are shown in (a,b) and (c), respectively. The narrow and broad black bars represent $\pi/2$ and π-pulses, respectively. The acquisition of the FIDs (indicated with the vertical dashed line) starts after (a) the end of the RN$_n^\nu$ block or (b) on top of the echo shifted with $\tau_R/2$ with respect to the end of the last recoupling block.

II. Pulse sequences and theory

110 **II.1. PRESTO**

II-1-1. Single-quantum hetero-nuclear dipolar recoupling

A RN$_n^\nu$ sequence, where N is an even positive integer and n and ν are integers, consists of $N/2$ pairs of elements $\mathcal{R}_\phi \mathcal{R}'_{-\phi}$ with $\mathcal{R}$ an inversion pulse with a duration of nT_R/N, where $T_R = 1/\nu_R = 2\pi/\omega_R$ is the rotor period, $\mathcal{R}'$ an inversion pulse derived from $\mathcal{R}$ by changing the sign of all phases and $\phi = \pi\nu/N$ radians an overall phase shift. The rf-field requirement of RN$_n^\nu$ is equal

115 to:

$$\nu_1 = \frac{N}{n}\frac{\xi^{tot}}{2\pi}\nu_R \tag{1}$$

where $\xi^{tot} = \sum_{i=1}^{P}\xi^i$ is the sum of the flip angles of the P individual pulses of the $\mathcal{R}$ element.

In the PRESTO sequence (Fig.1a), symmetry-based γ-encoded RN$_n^\nu$ schemes applied to the ^{1}H channel reintroduce the $|m| = 2$ space components and the single-quantum (SQ) terms of the hetero-nuclear dipolar couplings between the protons and the

120 quadrupolar nuclei, as well as the ^{1}H CSA, while they suppress the contributions of ^{1}H isotropic chemical shifts, the hetero-nuclear *J*-couplings with protons, and the ^{1}H-^{1}H dipolar couplings to the first-order average Hamiltonian.(Zhao et al., 2004) The hetero-nuclear dipolar interaction is characterized by a space rank l and a spin rank λ. A γ-encoded $|m| = 2$ SQ hetero-

nuclear dipolar recoupling must selectively reintroduce the two components $\{l, m, \lambda, \mu\} = \{2, 2, 1, \mu\}$ and $\{2, -2, 1, -\mu\}$ of the hetero-nuclear dipolar coupling and ^1H CSA with $\mu = \pm1$, while other components must be suppressed.

125 During these recoupling schemes, the contribution of the dipolar coupling between $I = {}^1H$ and S nuclei to the first-order Hamiltonian is equal to:(Zhao et al., 2004)

$$\bar{H}_{D,IS}^{(1)} = \omega_{D,IS} S_z [I^+ \exp(i2\varphi) + I^- \exp(-i2\varphi)], \tag{2}$$

where $I^\pm = I_x \pm iI_y$ are the shift operators, and the magnitude and phase of the recoupled I-S dipolar coupling are given by

$$\omega_{D,IS} = -\kappa \frac{\sqrt{3}}{2} b_{IS} \sin^2(\beta_{PR}^{D,IS}) \tag{3}$$

130 and

$$\varphi = \gamma_{PR}^{D,IS} - \omega_R t^0, \tag{4}$$

respectively, where b_{IS} is the dipolar coupling constant in rad/s, and κ is the scaling factor of the recoupled hetero-nuclear dipolar interaction, which depends on the RN_n^ν symmetry and the $\mathcal{R}$ element. The Euler angles $\{0, \beta_{PR}^{D,IS}, \gamma_{PR}^{D,IS}\}$ relate the I-S vector to the MAS rotor frame, and t^0 refers to the starting time of the recoupling. The norm of $\bar{H}_{D,IS}^{(1)}$ does not depend on the

135 $\gamma_{PR}^{D,IS}$ angle, since these recoupling schemes are γ-encoded.(Pileio et al., 2007; Martineau et al., 2012) The Hamiltonian of Eq.2 does not commute among different spin-pairs, and therefore the PRESTO sequence is affected by dipolar truncation, *i.e.*, the transfer to distant nuclei is attenuated by the stronger couplings with nearby spins.

As mentioned above, the SQ hetero-nuclear dipolar recoupling schemes also reintroduce the ^1H CSA with the same scaling factor κ, but without commuting with the recoupled ^1H-S dipolar interactions. Therefore, in the case of large ^1H CSA, for

140 instance at high magnetic fields, this interaction can interfere with the ^1H-S dipolar couplings, especially with small ones. These interferences can be limited by the use of the PRESTO-III variant, depicted in Fig.1a,c,(Zhao et al., 2004) in which three CT-selective pulses are applied to the S nucleus. Indeed, the CT-selective π-pulses partly refocus the ^1H CSA, which limits these interferences.

145 **II-1-2. Selection of the recoupling sequence**

On the basis of the AH and numerical simulations of spin dynamics, $R18_1^7$ and $R18_2^5$ schemes built from single rectangular π-pulses were selected for hetero-nuclear dipolar recoupling at moderate MAS frequencies, $\nu_R \approx 10$ kHz,(Zhao et al., 2001) while more recently, sequences based on symmetries $R12_5^4$, $R14_6^5$, $R16_7^5$, $R14_8^5$, $R18_8^7$, $R16_9^6$, $R20_9^8$ and $R18_{10}^7$ using 270_090_{180} as inversion element were chosen for the measurement of ^1H CSA at fast MAS frequencies, $\nu_R \approx 60$-70 kHz.(Pandey et al., 2015)

150 We also transferred the proton polarization to ^{27}Al nuclei at $\nu_R = 62.5$ kHz using PRESTO with $R16_3^2$ recoupling built from a single rectangular π-pulse.(Giovine et al., 2019a)

We screened here the RN_n^ν schemes built from single rectangular and composite π-pulses to achieve γ-encoded $|m| = 2$ SQ hetero-nuclear dipolar recoupling at $\nu_R = 20$ or 62.5 kHz. Dipolar recoupling at $\nu_R \geq 60$ kHz is useful to correlate the signals

of quadrupolar nuclei with high-resolution ^{1}H spectra without using homo-nuclear dipolar decoupling. We tested the following

155 composite π-pulses: $270_0 90_{180}$ with $\xi^{tot}/(2\pi) = 2$, which is offset-compensated and amplitude modulated and has been employed in several RN_n^ν sequences,(Giovine et al., 2019a; Carravetta et al., 2000; Levitt, 2002; Pandey et al., 2015) $90_0 240_{90} 90_0$ with $\xi^{tot}/(2\pi) = 7/3$, which compensates both rf inhomogeneity and offset,(Freeman et al., 1980; Duong et al., 2019) and $90_{-45} 90_{45} 90_{-45}$ with $\xi^{tot}/(2\pi) = 3/2$, which has homo-nuclear decoupling properties.(Madhu et al., 2001) Adiabatic pulses cannot be employed for SQ hetero-nuclear dipolar recoupling since they yield vanishing scaling factors for the rotational components

160 with $\mu \neq 0$.(Nagashima et al., 2018)

A total of 109 RN_n^ν symmetries with $2 \leq N \leq 30$, $2 \leq n \leq 7$ and $1 \leq \nu \leq 11$ were found which recouple {2, ±2, 1, ±1} or {2, ∓2, 1, ±1} rotational components of the ^{1}H-S dipolar coupling and ^{1}H CSA. We selected the RN_n^ν recouplings based on those symmetries with rf-field limited to $\nu_1 \leq 120$ and 190 for $\nu_R = 20$ and 62.5 kHz, respectively. As the currently employed γ-encoded $|m| = 2$ SQ hetero-nuclear dipolar recoupling schemes have $50° \leq \phi \leq 70°$, we only considered RN_n^ν symmetries with

165 $45° \leq \phi \leq 135°$. The scaling factor, κ, of the recoupled ^{1}H-S dipolar interaction was calculated using the 'C and R symmetries' Mathematica package.(Carravetta et al., 2000; Brinkmann and Levitt, 2001; Brinkmann et al., 2000; Brinkmann and Edén, 2004)

These RN_n^ν symmetries eliminate the contribution of ^{1}H-^{1}H dipolar interactions to the first-order Hamiltonian, but not their contribution to the second-order. The cross-terms between ^{1}H-^{1}H interactions in the second-order Hamiltonian can be

170 written(Brinkmann and Edén, 2004)

$$\bar{H}^{(2),DD_1 \times DD_2} = \frac{1}{\nu_R} \sum_{\{1,2\}} \kappa_{\{1,2\}}^{DD_1 \times DD_2} \left[A_{l_2 m_2}^{DD_2}\right]^R \left[A_{l_1 m_1}^{DD_1}\right]^R \exp[i(m_1 + m_2)\omega_R t^0] \left[T_{\lambda_2 \mu_2}^{DD_2}, T_{\lambda_1 \mu_1}^{DD_1}\right] \tag{5}$$

where the sum is taken over all second-order cross-terms {1,2} between the {l_1, m_1, λ_1, μ_1} and {l_2, m_2, λ_2, μ_2} rotational components of DD$_1$ and DD$_2$ ^{1}H-^{1}H dipolar interactions, respectively.

$\kappa_{\{1,2\}}^{DD_1 \times DD_2}$ is the scaling factor of this cross-term, $\left[A_{l_i m_i}^{DD_i}\right]^R$ and $T_{\lambda_i \mu_i}^{DD_i}$ denote the component m_i of the l_i^{th} rank spatial irreducible

175 spherical tensor A^{DD_i} in the MAS rotor-fixed frame and the component μ_i of the λ_i^{th} rank spin irreducible spherical tensor operator T^{DD_i}. Eq.5 indicates that the amplitude of the second-order Hamiltonian decreases at higher MAS frequency. The magnitude of the cross-terms between ^{1}H-^{1}H interactions was estimated by calculating the Euclidean norm(Hu et al., 2009; Gansmüller et al., 2013)

$$\left\| \kappa_{\{1,2\}}^{DD_1 \times DD_2} \right\|_2 = \sqrt{\sum_{\{1,2\}} \left| \kappa_{\{1,2\}}^{DD_1 \times DD_2} \right|^2}. \tag{6}$$

180 For each basic element $\mathcal{R}$, we selected the RN_n^ν schemes with the highest ratio $\kappa / \left\| \kappa_{\{1,2\}}^{DD_1 \times DD_2} \right\|_2$ in order to minimize the interference of ^{1}H-^{1}H dipolar interactions with the ^{1}H-S dipolar recoupling. Besides ^{1}H-^{1}H dipolar interactions, other cross-terms involving ^{1}H CSA and offset can also interfere with the ^{1}H-S dipolar recoupling. These cross-terms can be expressed by Eq.5, in which DD$_1$ and DD$_2$ indexes are substituted by other interactions, such as ^{1}H CSA or isotropic chemical shift (δ_{iso}).

For the selected symmetries, we estimated the magnitude of the cross-terms between ^{1}H CSA or offset by calculating the
Euclidean norms $\left\|\kappa_{\{1,2\}}^{CSA \times CSA}\right\|_2$ and $\left\|\kappa_{\{1,2\}}^{\delta iso \times \delta iso}\right\|_2$ given by Eq.6.

The corresponding selected RN_n^ν sequences are listed in Table 1 for $\nu_R = 20$ kHz and Table 2 for $\nu_R = 62.5$ kHz.

For $\nu_R = 20$ kHz, according to the AH, the RN_n^ν sequence with the highest robustness to ^{1}H-^{1}H dipolar interactions is
$R22_2^7(180_0)$. However, this recoupling is slightly less robust to ^{1}H CSA and offset than $R18_2^5(180_0)$, which has already been
reported. For this MAS frequency, the RN_n^ν schemes using the chosen composite pulses either required rf-fields greater than
120 kHz, e.g. $\nu_1 = 130$ and 173 kHz for the $R26_3^7$ schemes built from $90_{-45}90_{45}90_{-45}$ and 270_090_{180} pulses, or did not suppress
efficiently the second-order cross-terms between ^{1}H-^{1}H interactions because of small rf-field ($\nu_1 \leq 62.5$ kHz).

Table 1. Selected RN_n^ν $|m| = 2$ SQ hetero-nuclear dipolar recoupling for $\nu_R = 20$ kHz.

$\mathcal{R}$	RN_n^ν	$\phi°$	ν_1/ν_R	κ	$\kappa/\left\|\kappa_{\{1,2\}}^{DD_1 \times DD_2}\right\|_2$	$\kappa/\left\|\kappa_{\{1,2\}}^{CSA \times CSA}\right\|_2$	$\kappa/\left\|\kappa_{\{1,2\}}^{\delta iso \times \delta iso}\right\|_2$
	$R22_2^7$	57	5.5	0.178	162	7.12	17.58
180_0	$R28_3^5$	51	4.67	0.176	156	5.08	18.29
	$R18_2^5$	50	4.5	0.175	140	7.20	18.49

For $\nu_R = 62.5$ kHz, the RN_n^ν sequences using composite π-pulses recouple the ^{1}H-S dipolar interaction with a higher scaling
factor than those built from single π-pulses. According to AH, the $90_0240_{90}90_0$ basic element leads to the highest robustness
to ^{1}H-^{1}H interferences. Even if the amplitude of the cross-terms is inversely proportional to the MAS frequency (Eq.5), the
amplitude of these terms is lower at $\nu_R = 20$ than 62.5 kHz. The 270_090_{180} element is less robust to ^{1}H-^{1}H interferences, but
benefits from a high robustness to offset. The selected RN_n^ν symmetries for this element include $R14_6^5$ and $R16_7^6$, which have
already been employed for the measurement of ^{1}H CSA and the transfer of ^{1}H polarization to half-integer quadrupolar nuclei
at $\nu_R \geq 60$ kHz.(Giovine et al., 2019a; Pandey et al., 2015) As the scaling factors κ of the ^{1}H-S dipolar interaction of the RN_n^ν
schemes built from single π-pulses with $45° \leq \phi \leq 135°$ are small, we also selected in Table 3 RN_n^ν schemes built from single
π-pulses with $\kappa \geq 0.15$, but with extended ϕ ranges. These recoupling schemes are less robust to offset than the RN_n^ν schemes
built from 270_090_{180} element.

Table 2. Selected RN_n^ν $|m| = 2$ SQ hetero-nuclear dipolar recoupling with $45° \leq \phi \leq 135°$ for $\nu_R = 62.5$ kHz.

$\mathcal{R}$	RN_n^ν	$\phi°$	ν_1/ν_R	κ	$\kappa/\left\|\kappa_{\{1,2\}}^{DD_1 \times DD_2}\right\|_2$	$\kappa/\left\|\kappa_{\{1,2\}}^{CSA \times CSA}\right\|_2$	$\kappa/\left\|\kappa_{\{1,2\}}^{\delta iso \times \delta iso}\right\|_2$
	$R10_4^3$	54	2.92	0.227	39.63	2.82	12.63
$90_0240_{90}90_0$	$R14_6^5$	64.3	2.72	0.232	36.33	1.87	12.39

	$\mathrm{R}12_5^4$	60	2.80	0.230	36.08	2.25	12.47
	$\mathrm{R}12_7^8$	120	2.00	0.227	35.96	1.61	7.72
	$\mathrm{R}16_7^6$	67.5	2.28	0.150	17.96	1.85	3.50×10^{10}
$270_0 90_{180}$	$\mathrm{R}16_7^{10}$	112.5	2.28	0.150	17.96	1.85	3.50×10^{10}
	$\mathrm{R}14_6^5$	64.3	2.33	0.150	15.90	2.33	3.58×10^{10}
	$\mathrm{R}14_6^9$	115.7	2.33	0.150	15.90	2.15	3.58×10^{10}
	$\mathrm{R}10_4^3$	54	1.88	0.186	16.70	2.97	15.07
$90_{-45} 90_{45} 90_{-45}$	$\mathrm{R}18_7^5$	50	1.93	0.189	15.73	1.98	25.49
	$\mathrm{R}14_6^5$	64.3	1.75	0.177	15.55	2.09	5.49
	$\mathrm{R}12_5^4$	60	1.80	0.181	15.17	2.47	8.11
	$\mathrm{R}14_6^5$	64.3	1.16	0.085	5.35	2.26	1.34
180_0	$\mathrm{R}14_6^9$	115.7	1.16	0.085	5.35	2.26	1.34
	$\mathrm{R}16_7^6$	67.5	1.14	0.082	4.90	1.98	1.09
	$\mathrm{R}16_7^{10}$	112.5	1.14	0.082	4.90	1.98	1.09

Table 3. Selected $\mathrm{R}N_n^\nu$ $|m| = 2$ SQ hetero-nuclear dipolar recoupling built from single π pulses with $20° \leq \phi \leq 160°$ and $\kappa \geq 0.15$ for $\nu_R = 62.5$ kHz.

$\mathcal{R}$	$\mathrm{R}N_n^\nu$	ϕ /°	ν_1/ν_R	κ	$\kappa / \left\| \kappa_{\{1,2\}}^{DD_1 \times DD_2} \right\|_2$	$\kappa / \left\| \kappa_{\{1,2\}}^{CSA \times CSA} \right\|_2$	$\kappa / \left\| \kappa_{\{1,2\}}^{\delta iso \times \delta iso} \right\|_2$
	$\mathrm{R}28_5^4$	25.7	2.75	0.163	24.42	3.34	26.42
180_0	$\mathrm{R}22_4^3$	24.5	2.75	0.162	22.84	4.10	27.24
	$\mathrm{R}16_3^2$	22.5	2.67	0.161	16.26	5.21	28.89

II-2. *D*-RINEPT

II-2-1. Zero-quantum hetero-nuclear dipolar recoupling

In the *D*-RINEPT sequence, the ¹H-*S* dipolar interactions are reintroduced under MAS by applying non-γ-encoded two-spin order dipolar recoupling to the ¹H channel. These recoupling schemes reintroduce the $|m| = 2$ space components and the zero-quantum (0Q) terms of the ¹H-*S* dipolar interaction and ¹H CSA, *i.e.,* the rotational components $\{l, m, \lambda, \mu\} = \{2, \pm 2, 1, 0\}$, while they suppress the contributions of ¹H isotropic chemical shifts, the hetero-nuclear *J*-couplings with protons, and the ¹H-¹H dipolar couplings to the first-order average Hamiltonian.(Brinkmann and Kentgens, 2006a, b) The contribution of the ¹H-*S* dipolar coupling to this Hamiltonian is equal to:(Giovine et al., 2019a; Brinkmann and Kentgens, 2006a; Lu et al., 2012)

$$\bar{H}_{D,IS}^{(1)} = 2\omega_{D,IS}I_z S_z \tag{7}$$

where

$$\omega_{D,IS} = \kappa b_{IS}\sin^2\left(\beta_{PR}^{D,IS}\right)\cos(2\varphi), \tag{8}$$

The norm of $\bar{H}_{D,IS}^{(1)}$ depends on the φ phase, given by Eq.4, and hence on the $\gamma_{PR}^{D,IS}$ angle. Therefore, these two-spin order dipolar

225 recoupling schemes are non-γ-encoded. The Hamiltonian of Eq.7 commutes among different spin pairs and hence, these recoupling schemes are not affected by dipolar truncation. Similarly, the recoupled ^{1}H CSA contribution to the first-order Hamiltonian is proportional to I_z and hence, commutes with the recoupled ^{1}H-S dipolar interactions and does not interfere with the hetero-nuclear dipolar recoupling.

II-2-2. Selection of the recoupling sequence

230 Different RN_n^ν sequences have been proposed to achieve non-γ-encoded $|m| = 2$ two-spin order dipolar recoupling, including (i) symmetries R$(4n)_n^{2n-1}$ = R12_3^5, R16_4^7, R20_5^9, R24_6^{11}, R28_7^{13} and R32_8^{15} for n = 3, 4, 5, 6, 7 and 8 using single π-pulses as basic element, which have been employed to measured ^{1}H-^{17}O dipolar couplings at ν_R = 50 kHz,(Brinkmann and Kentgens, 2006b) (ii) SR4_1^2 recoupling built from a single π-pulse, which corresponds to the $[R4_1^2R4_1^{-2}]_0[R4_1^2R4_1^{-2}]_{120}[R4_1^2R4_1^{-2}]_{240}$ sequence and has been employed in the RINEPT scheme,(Nagashima et al., n.d.; Giovine et al., 2019a) (iii) R12_3^5 and SR4_1^2

235 schemes using a $90_{-45}90_{45}90_{-45}$ composite π-pulse as a basic element, which have been incorporated into D-HMQC sequences at ν_R = 36 kHz,(Perras et al., 2019) and (iv) SR4_1^2 schemes built from a tanh/tan adiabatic pulse, which have been used in RINEPT sequence at $\nu_R \approx$ 36 kHz.(Nagashima et al., 2020, n.d.) During the tanh/tan pulse, the instantaneous rf-amplitude is equal to:

$$\omega_1(t) = \omega_{1,max}\begin{cases} \tanh\left[\frac{8\xi t}{T_R}\right] & 0 \le t < T_R/8 \\ \tanh\left[2\xi\left(1 - \frac{4t}{T_R}\right)\right] & T_R/8 \le t < T_R/4 \end{cases} \tag{9}$$

240 where $\omega_{1,max}$ is the peak amplitude of the rf-field, t refers to the time since the start of the pulse, which lasts $T_R/4$ when incorporated into the SR4_1^2 recoupling scheme. The parameter ξ determines the rise and fall times of the pulse. Hence, in the frequency-modulated (FM) frame,(Garwood and DelaBarre, 2001) the frequency offset i

$$\phi_I(t) = \frac{\Delta\nu_{0,max}}{2\theta\tan(\theta)}\ln\left\{\cos\left[\theta\left(1 - 8\frac{t}{T_R}\right)\right]\right\}. \tag{10}$$

where $\Delta\nu_{0,max}$ is the peak amplitude of the carrier frequency modulation and θ determines the frequency sweep rate in the

245 center of the pulse. Here, we employed $\xi = 10$ and $\theta = 87° = $ atan(20).(Nagashima et al., 2020; Kervern et al., 2007; Nagashima et al., 2018)

We screened here the RN_n^ν schemes built from 180_0, 270_090_{180}, $90_0240_{90}90_0$ and $90_{-45}90_{45}90_{-45}$ elements. A total of 58 RN_n^ν symmetries with $2 \le N \le 30$, $2 \le n \le 7$ and $1 \le \nu \le 11$ were found which recouple the {2, ±2, 1, 0} rotational components of

the ^{1}H-S dipolar coupling and ^{1}H CSA. We only considered the RN_n^{ν} symmetries with $60° \leq \phi \leq 120°$ since the currently
250   employed non-γ-encoded $|m| = 2$ two-spin order hetero-nuclear dipolar recoupling schemes have $75° \leq \phi \leq 90°$.

    We calculated the scaling factor of the recoupled ^{1}H-S dipolar interaction and the Euclidean norm and $\left\| \kappa_{\{1,2\}}^{DD_1 \times DD_2} \right\|_2$ of the cross-terms between ^{1}H-^{1}H interactions using the 'C and R symmetries' Mathematica package.(Carravetta et al., 2000; Brinkmann and Levitt, 2001; Brinkmann et al., 2000; Brinkmann and Edén, 2004) For each basic element $\mathcal{R}$, we selected the RN_n^{ν} schemes with the highest ratios $\kappa / \left\| \kappa_{\{1,2\}}^{DD_1 \times DD_2} \right\|_2$. The selected R$N_n^{\nu}$ sequences are listed in Table 4. The parameters of the
255   SR4$_1^2$ schemes built from the different basic element $\mathcal{R}$ are also listed in Table 4 for the sake comparison. For those RN_n^{ν} sequences, we calculated the Euclidean norms $\left\| \kappa_{\{1,2\}}^{CSA \times CSA} \right\|_2$ and $\left\| \kappa_{\{1,2\}}^{\delta iso \times \delta iso} \right\|_2$ in order to estimate the magnitudes of the cross-terms between ^{1}H CSA and offset.

    According to the AH, the $90_0 240_{90} 90_0$ composite π-pulse yields the highest robustness to ^{1}H-^{1}H dipolar interactions. However, the rf-field requirement of the RN_n^{ν} sequences built from this composite pulse, $\nu_1 = 4.66 \nu_R$, $i.e.$, $\nu_1 = 291$ kHz at $\nu_R = 62.5$ kHz,
260   is not compatible with most 1.3 mm MAS probes. Furthermore, the highest robustness to ^{1}H CSA and offset is achieved using the $270_0 90_{180}$ composite π-pulse. The SR4$_1^2$ schemes benefit from the highest robustness to ^{1}H CSA, because of the three-step multiple-quantum super-cycle.(Brinkmann and Edén, 2004; Brinkmann and Kentgens, 2006a) Contrary to the RN_n^{ν} $|m| = 2$ SQ hetero-nuclear dipolar recouplings, the rf-field of the RN_n^{ν} $|m| = 2$ two-spin orders is always higher than $2\nu_R$ since these RN_n^{ν} symmetries with $2n > N$, such as R12$_9^5$, lead to vanishing κ scaling factor.
265   In the case of the adiabatic RN_n^{ν} (tt) sequences, the determination of the scaling factors of first- and second-order terms of the effective Hamiltonian is more cumbersome since they depend on the $\nu_{1,max}$, $\Delta\nu_{0,max}$, ξ and θ parameters.(Nagashima et al., 2018) For example, the scaling factor of the R12$_3^5$ and SR4$_1^2$ schemes is $\kappa = 0.31$ for $\nu_{1,max}/\Delta\nu_{0,max} = 0.685$, $\xi = 10$ and $\theta = 87°$, and this value monotonously decreases for increasing $\nu_{1,max}/\Delta\nu_{0,max}$ ratios.

270   **Table 4. Selected RN_n^{ν} $|m| = 2$ two-spin order hetero-nuclear dipolar recoupling.**

$\mathcal{R}$	RN_n^{ν}	$\phi°$	ν_1/ν_R	κ	$\kappa / \left\| \kappa_{\{1,2\}}^{DD_1 \times DD_2} \right\|_2$	$\kappa / \left\| \kappa_{\{1,2\}}^{CSA \times CSA} \right\|_2$	$\kappa / \left\| \kappa_{\{1,2\}}^{\delta iso \times \delta iso} \right\|_2$
	R16$_4^9$	101	4.66	0.131	63.17	16.48	9.31
	R20$_5^{11}$	99	4.66	0.131	60.68	16.59	14.45
	R12$_3^7$	105	4.66	0.131	51.25	16.11	9.70
$90_0 240_{90} 90_0$	R16$_4^7$	79	4.66	0.131	45.52	15.76	13.60
	R28$_7^{10}$	64	4.66	0.131	44.55	14.06	11.98
	R20$_5^9$	81	4.66	0.131	44.30	15.95	14.46
	R12$_3^5$	75	4.66	0.131	43.91	15.40	12.83

	SR4$_1^2$	90	4.66	0.131	42.37	22.65	10.48
	R28$_7^{11}$	71	3	0.191	39.81	10.05	6.10
	R20$_5^8$	72	3	0.191	39.74	10.26	5.49
	R8$_2^3$	67.5	3	0.191	39.43	9.42	7.88
$90_{-45}90_{45}90_{-45}$	R8$_2^{11}$	67.5	3	0.191	39.43	9.42	7.88
	R24$_6^{10}$	75	3	0.191	39.32	10.66	4.22
	R28$_7^{10}$	64.3	3	0.191	38.82	8.65	10.13
	R12$_3^5$	75	3	0.191	38.33	10.66	4.22
	SR4$_1^2$	90	3	0.191	19.95	19.48	1.33
	R24$_6^{11}$	82.5	4	0.212	33.12	25.46	8.67×10^{10}
	R20$_5^9$	81	4	0.212	31.85	25.19	8.67×10^{10}
	R20$_5^{11}$	99	4	0.212	31.85	25.19	8.67×10^{10}
$270_0 90_{180}$	R16$_4^7$	78.8	4	0.212	28.56	24.69	8.67×10^{10}
	R16$_4^9$	101.2	4	0.212	28.56	24.69	8.67×10^{10}
	R12$_3^5$	75	4	0.212	20.84	23.58	8.67×10^{10}
	R12$_3^7$	105	4	0.212	20.84	23.58	8.67×10^{10}
	SR4$_1^2$	90	4	0.212	35.21	149.93	8.67×10^{10}
	R16$_4^7$	78.8	2	0.25	19.65	10.52	2.78
	R16$_4^9$	115.7	2	0.25	19.65	10.52	2.78
180_0	R12$_3^5$	75	2	0.25	18.9	9.89	3.74
	R12$_3^7$	105	2	0.25	18.9	9.89	3.74
	SR4$_1^2$	90	2	0.25	13.2	22.98	1.56

II-2-3. _D_-RINEPT-CWc sequence

The _D_-RINEPT-CWc sequence is displayed in Fig.1b,c. The ^{1}H-S dipolar couplings are reintroduced by applying the RN_n^ν schemes listed in Table 4 during the defocusing and refocusing delays τ, which are identical in this article, even if distinct defocusing and refocusing delays can improve the transfer efficiency.(Nagashima et al., 2020) As the two-spin order recoupling schemes are non-γ-encoded, they must be rotor-synchronized. We used here a delay of T_R between two successive RN_n^ν blocks. In the _D_-RINEPT-CWc sequence, a CW irradiation is applied during these delays in order to limit the losses due to ^{1}H-^{1}H dipolar interactions.(Nagashima et al., n.d.) The nutation during this CW irradiation is eliminated by employing CW irradiations with opposite phases. Furthermore, the robustness to ^{1}H rf-field inhomogeneity is improved by replacing the first

280 π and second π/2 pulses by composite $90_0180_{90}90_0$ and $90_{90}90_0$ pulses, respectively, the CW irradiation being applied between the individual pulses.(Freeman et al., 1980; Levitt and Freeman, 1979)

III. Numerical simulations

III-1. Simulation parameters

All simulations were performed using the version 4.1.1 of SIMPSON package (Bak et al., 2000, p.200). The powder average
285 calculation was performed using 462 {α_{MR}, β_{MR}, γ_{MR}} Euler angles relating the rotor and molecular frames. This set of angles was obtained by considering 66 {α_{MR}, β_{MR}} pairs and 7 γ_{MR} angles. The {α_{MR}, β_{MR}} values were selected according to the REPULSION algorithm (Bak and Nielsen, 1997b), while the γ_{MR} angles were regularly stepped from 0 to 360°.

To accelerate the simulations, the $^1H\rightarrow$ ^{15}N RINEPT transfer was used, instead of the $^1H\rightarrow$ ^{27}Al one, because the computing time is proportional to the cube of the size of the density matrix. Furthermore, in RINEPT experiments, only CT-selective
290 pulses are applied to the quadrupolar nuclei and hence, the contribution of STs to the signal can be disregarded. The $^1H\rightarrow^{15}N$ RINEPT transfer was simulated for a $^{15}N^1H_4$ spin system. A similar approach has already been applied for the simulation of the RINEPT transfer from protons to quadrupolar nuclei (Nagashima et al., n.d.; Giovine et al., 2019b). This $^{15}N^1H_4$ spin system comprises a tetrahedron of four protons with a ^{15}N nucleus on one of its symmetry axis. The dipolar coupling constants between protons are all equal to $|b_{HH}|/(2\pi) = 1$, 7 or 15 kHz. The dipolar coupling between ^{15}N nucleus and its closest ^1H
295 neighbor is $|b_{HN}|/(2\pi) = 2575$ Hz, corresponding to a ^1H-^{27}Al distance of 2.3 Å, typical of the distance between the protons of hydroxyl groups and the Al atoms of the first surface layer of hydrated γ-alumina (Lee et al., 2014). All protons were subject to a CSA of 6 kHz, *i.e.*, 7.5 ppm at 18.8 T, their asymmetry parameters were null, and their principal axis coincide with the 3-fold rotational axes of the $^1H_4$ tetrahedron.

The simulations were performed for a static magnetic field of 18.8 T, for which the ^1H and ^{15}N Larmor frequencies were equal
300 to 800 and 81 MHz, respectively using MAS frequencies of $\nu_R = 20$ or 62.5 kHz (Liang et al., 2018). $^1H\rightarrow$ ^{15}N RINEPT-CWc sequences incorporating either $SR4_1^2$(tt) or $R12_3^5$(tt) recoupling schemes were simulated. The defocusing and refocusing periods were both equal to their optimal values τ = 650 or 640 μs at $\nu_R = 20$ or 62.5 kHz, respectively. The rf-field nutation frequency on the ^1H channel was equal to 200 kHz during the π/2 and π-pulses, which do not belong to the recoupling sequence, as well as the CW irradiation, whereas the pulses applied to $S = {}^{15}N$ nuclei were considered as ideal Dirac pulses. Simulations
305 were performed for recoupling schemes made of tanh/tan adiabatic pulses with $\nu_{1,max}$ and $\Delta\nu_{0,max}$ parameters ranging from $0.5\nu_R$ to $10\nu_R$ and from $10\nu_R$ to $200\nu_R$, respectively. The other pulses were applied on resonance. The density matrix before the first pulse was equal to $I_{1z} + I_{2z} + I_{3z} + I_{4z}$. We normalized the transfer efficiency of $^1H\rightarrow$ ^{15}N RINEPT sequences to the maximal signal for a $^1H\rightarrow$ ^{15}N through-bond RINEPT sequence made of ideal Dirac pulses in the case of a ^{15}N-^1H spin system with a *J*-coupling constant of 150 Hz.

310
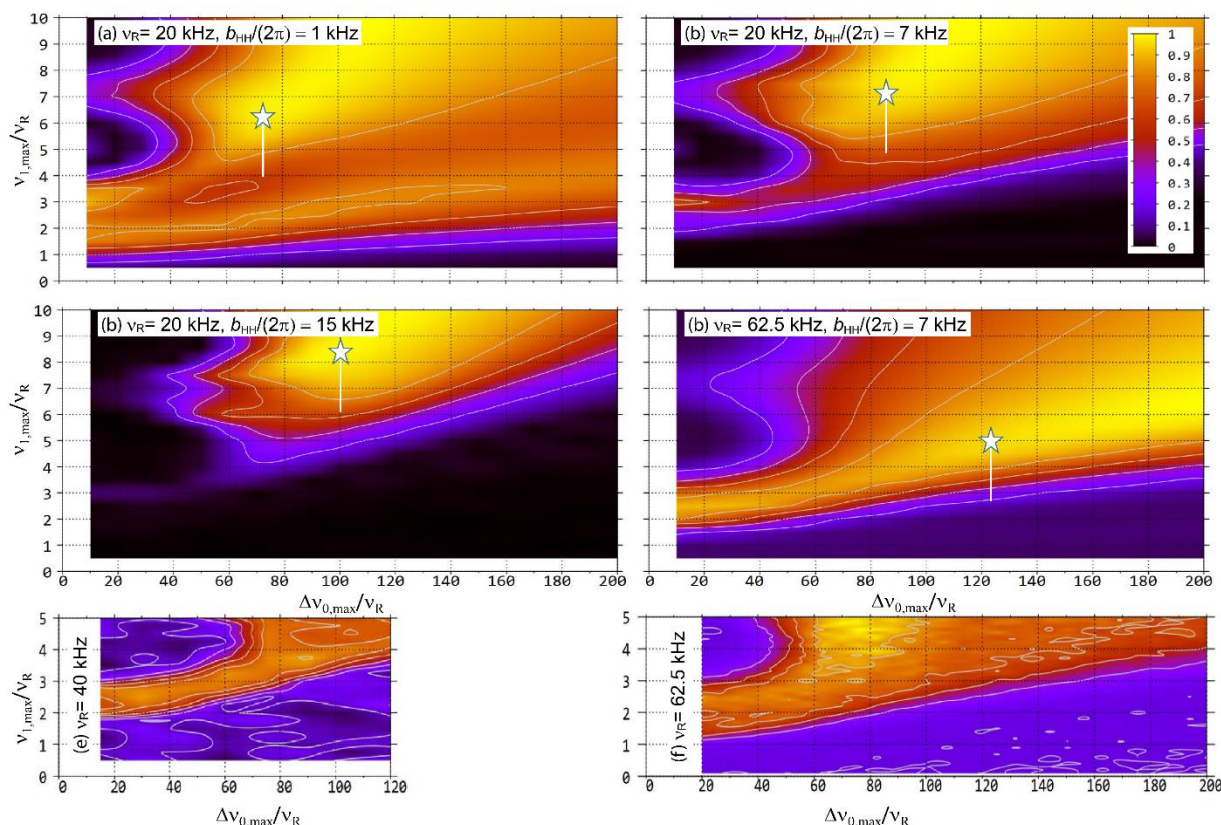
Figure 2: (a-d) Simulated transfer efficiency of $^1H \rightarrow \,^{15}N$ D-RINEPT-SR4$_1^2$(tt) sequence for a $^{15}N^1H_4$ spin system as function of $\nu_{1,max}/\nu_R$ and $\Delta\nu_{0,max}/\nu_R$ for ν_R = 20 and 62.5 kHz and $b_{HH}/(2\pi)$ = **(a)** 1, **(b,d)** 7 and **(c)** 15 kHz. **(e,f)** Experimental $^1H \rightarrow \,^{15}N$ D-RINEPT-SR4$_1^2$(tt) signal of L-histidine·HCl as function of $\nu_{1,max}/\nu_R$ and $\Delta\nu_{0,max}/\nu_R$ at 18.8 T with ν_R = **(e)** 40 **(e)** or **(f)** 62.5 kHz. The white star indicates recoupling conditions with minimal rf field leading to maximal transfer efficiency. The white vertical line mimics the rf-field distribution within the coil.

III-2. Optimal adiabatic recoupling

The transfer efficiency of RINEPT using RN_n^ν schemes built from adiabatic pulses, depends on $\nu_{1,max}$ and $\Delta\nu_{0,max}$ parameters. For a similar $^{15}N^1H_4$ spin system with $|b_{HN}|/(2\pi)$ = 2.575 and $|b_{HH}|/(2\pi)$ = 7 kHz, spinning at ν_R = 12.5 kHz, we showed using numerical simulations of spin dynamics that a maximal transfer efficiency was achieved provided that $\nu_{1,max} = 0.07\Delta\nu_{0,max}$ and $\nu_{1,max}/\nu_R \geq 8$.(Nagashima et al., n.d.) In practice, we used $\nu_{1,max} = 11\nu_R = 137$ kHz and $\Delta\nu_{0,max} = 160\nu_R = 2$ MHz.

Similar simulations were performed here for ν_R = 20 or 62.5 kHz. As seen in Fig.2a-c, at a given MAS frequency, higher ^1H-^1H dipolar couplings require higher rf-field and broader carrier frequency sweep so that the tanh/tan pulses remain adiabatic in spite of the modulation of the ^1H-^1H dipolar couplings by MAS.(Nagashima et al., n.d.; Kervern et al., 2007) For $|b_{HH}|/(2\pi)$ = 7 kHz, the minimal $\nu_{1,max}/\nu_R$ ratio decreases for higher MAS frequencies (compare Figs.2b and d) since the contribution of

the modulation of ^{1}H-^{1}H dipolar couplings by MAS to the first adiabaticity factor is proportional to $(\nu_{1,max})^2/\nu_R$ and hence, $\nu_{1,max}$ values proportional to $\sqrt{\nu_R}$, i.e. $\nu_{1,max}/\nu_R$ ratio inversely proportional to $\sqrt{\nu_R}$, are sufficient to maintain the adiabaticity of the pulses.(Kervern et al., 2007) Nevertheless, Fig.2d indicates that SR4$_1^2$(tt) recoupling requires $\nu_{1,max} \geq 313$ kHz for $\nu_R = 62.5$

330   kHz. This rf field is not compatible with the specifications of most 1.3 mm MAS probes. Similar transfer efficiencies were simulated for the RINEPT sequence with R12$_3^5$(tt) recoupling scheme (not shown).

IV. NMR experiments

IV-1. Samples and experimental conditions

L-[U-^{15}N]-histidine·HCl (hereafter referred to as "histidine") and isotopically unmodified γ-alumina were purchased from

335   Merck, and AlPO$_4$-14 was prepared as described previously.(Antonijevic et al., 2006)

All ^{1}H → S RINEPT-CWc and PRESTO-III experiments were performed at B$_0$ = 18.8 T on Bruker BioSpin Avance NEO spectrometers equipped with double-resonance ^{1}H/X probes.

^{1}H→^{15}N RINEPT-CWc experiments using SR4$_1^2$(tt) recoupling (denoted RINEPT-CWc-SR4$_1^2$(tt) hereafter) on histidine were performed with 1.3 and 0.7 mm MAS probes spinning at $\nu_R = 40$ or 62.5 kHz, with defocusing and refocusing delays equal to

340   $\tau = 375$ or 384 µs, respectively. The rf-field of the ^{1}H π/2 and π pulses, which do not belong to the recoupling scheme, was equal to 200 kHz, that of the continuous wave irradiation to $\nu_{1,CW} = 100$ kHz, and that of the ^{15}N pulses to 62 kHz. ^{1}H decoupling with a rf-field of 16 kHz was applied during the acquisition. The pulses on the ^{1}H channel were applied on resonance, whereas those on ^{15}N channel were applied at the isotropic chemical shift of the ^{15}NH$^\tau$ signal (172 ppm). These 1D spectra resulted from averaging 8 transients with a relaxation delay of 3 s. The ^{15}N isotropic chemical shifts were referenced to an aqueous

345   saturated solution of NH$_4$NO$_3$ using [^{15}N]-glycine as a secondary reference.

^{1}H→^{27}Al RINEPT-CWc and PRESTO-III experiments on γ-alumina and AlPO$_4$-14 were performed with a 1.3 mm MAS probe spinning at $\nu_R = 20$ (to test the RN_n^ν schemes with large rf-fields) or 62.5 kHz. The tested recoupling schemes are listed in Tables 5 and 6 for $\nu_R = 20$ kHz and Tables 7 and 8 for $\nu_R = 62.5$ kHz. The rf-field of the ^{1}H π/2 and π pulses, which do not belong to the recoupling scheme, was equal to 208 kHz, that of the continuous wave irradiation to $\nu_{1,CW} = 147$ kHz, and the

350   ^{27}Al CT-selective one for π/2 and π pulses to 10 kHz. The defocusing and refocusing delays τ are given in Table 5 to 8. The pulses on the ^{1}H channel were applied on resonance, whereas those on ^{27}Al channel were applied (i) on resonance with AlO$_6$ signal of γ-alumina in Figs.4 and 7, Tables 5 and 7, as well as in Figs. 5 and 8 when the offset is null, (ii) on resonance with AlO$_4$ signal of AlPO$_4$-14 in Figs.S1 and S3, Tables 6 and 8 as well as in Figs.S2 and S4 when the offset is null, and (iii) in the middle of the AlO$_4$ and AlO$_6$ peaks for the 1D spectra shown in Figs.3 and 6. These differences in offset explain some changes

355   in the relative efficiencies of the recoupling between the figures. These 1D spectra resulted from averaging 64 transients with a relaxation delay of 1 s The ^{27}Al isotropic chemical shifts were referenced at 0 ppm to 1 mol.L^{-1} [Al(H$_2$O)$_6$]$^{3+}$ solution.

MAGNETIC RESONANCE
Open Access Discussions

IV-2. Optimal adiabatic recoupling

Figs.**2e** and **f** show the efficiency of $^1H \rightarrow {}^{15}N$ RINEPT-SR4$_1^2$(tt) transfer for histidine as function of $\nu_{1,max}/\nu_R$ and $\Delta\nu_{0,max}/\nu_R$

360 for $\nu_R = 40$ or 62.5 kHz, respectively. These experimental data indicate that at higher MAS frequency, an efficient adiabatic recoupling can be achieved for lower $\nu_{1,max}/\nu_R$ and $\Delta\nu_{0,max}/\nu_R$ ratios. This result agrees with the numerical simulations of Figs.2b and d.
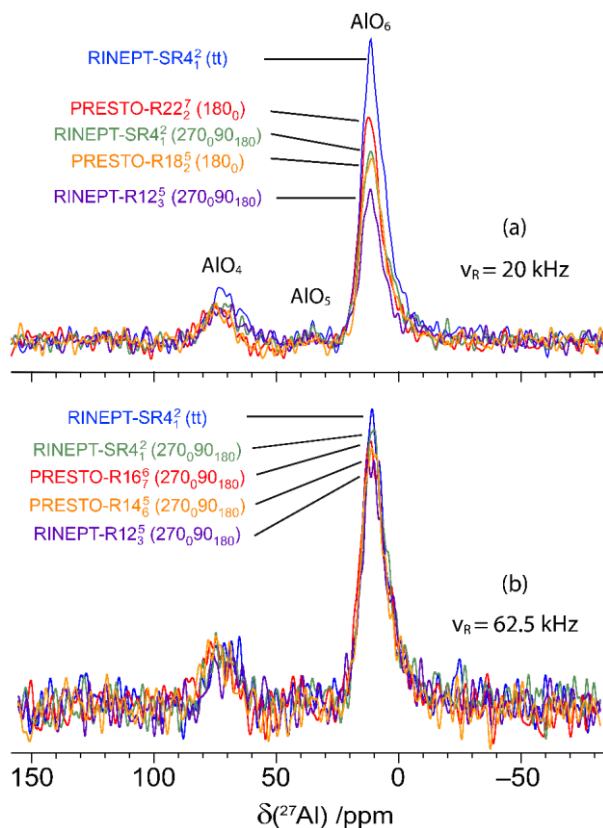
Figure 3: 1D ^{27}Al spectra of γ-alumina at B$_0$ = 18.8 T with ν_R = (a) 20 and (b) 62.5 kHz acquired using $^1H \rightarrow {}^{27}$Al RINEPT-CWc and PRESTO-III transfers using the following recoupling schemes: SR4$_1^2$(tt), SR4$_1^2$(270$_0$90$_{180}$) or R12$_3^5$ (270$_0$90$_{180}$) for RINEPT and
365 **R22$_2^7$(180$_0$) or R18$_2^5$ (180$_0$) for PRESTO at ν_R = 20 kHz, and R16$_7^6$ (270$_0$90$_{180}$) or R14$_6^5$ (270$_0$90$_{180}$) for PRESTO at ν_R = 62.5 kHz (b). τ delay and $\nu_1/\nu_{1,max}$ rf-field were fixed to their optimum values given in Tables 5 and 7.**

IV-3. PRESTO and RINEPT performances for ν_R = 20 kHz

IV-3-1. γ-alumina

370 The 1D NMR spectra of γ-alumina acquired using $^1H \rightarrow {}^{27}$Al RINEPT and PRESTO sequences, shown in Fig.3, exhibit two resonances at 70 and 10 ppm, assigned to tetra- (AlO$_4$) and hexa-coordinated (AlO$_6$) resonances, respectively.(Morris and

Ellis, 1989) The signal of penta-coordinated (AlO$_5$) sites, which are mainly located in the first surface layer, is barely detected because of the lack of sensitivity of conventional solid-state NMR spectroscopy.(Lee et al., 2014, p.201) The most intense peak, AlO$_6$, was used to compare the transfer efficiencies of RINEPT and PRESTO sequences with different recoupling

375   schemes.

Table 5 lists the measured performances of ^{1}H $\rightarrow$ ^{27}Al RINEPT-CWc and PRESTO transfers using various recoupling for γ-alumina at $v_R = 20$ kHz. We notably compared the PRESTO sequences using R22$_2^7$(180$_0$) and R18$_2^5$(180$_0$) recoupling (Table 1) with the RINEPT-CWc scheme using a recoupling based on SR4$_1^2$ and R12$_3^5$ symmetries with: single 180$_0$, composite 270$_0$90$_{180}$ and 90$_{-45}$90$_{45}$90$_{-45}$ or tanh/tan adiabatic pulses. A low transfer efficiency was obtained for RINEPT-CWc-

380   SR4$_1^2$(90$_0$240$_{90}$90$_0$) because of its low scaling factor $\kappa = 0.131$ and hence, its performances are not reported in Table 5. We also tested the recoupling schemes based on the symmetry SC4$_2^0$, corresponding to the [C4$_2^0$]$_0$[C4$_2^0$]$_{120}$[C4$_2^0$]$_{240}$ sequence with a basic element 90$_{45}$90$_{135}$90$_{45}$90$_{225}$90$_{315}$90$_{225}$, or C6$_3^0$ built from 90$_{30}$90$_{120}$90$_{30}$90$_{240}$90$_{330}$90$_{240}$. These recoupling schemes, which have been recently proposed,(Perras et al., 2019) derive from the SR4$_1^2$(90$_{-45}$90$_{45}$90$_{-45}$) and R12$_3^5$(90$_{-45}$90$_{45}$90$_{-45}$) schemes.

As seen in Table 5, the sequences yielding the highest transfer efficiencies are by decreasing order RINEPT-CWc with SR4$_1^2$(tt)

385   or R12$_3^5$ (tt) > PRESTO- R22$_2^7$ (180$_0$) > RINEPT-CWc- SR4$_1^2$ (270$_0$90$_{180}$) $\approx$ PRESTO- R18$_2^5$ (180$_0$) > RINEPT-CWc-R12$_3^5$(270$_0$90$_{180}$). Figs.4 and 5 display the signal intensity of these sequences as function of the rf-field amplitude and offset, respectively.

The highest transfer efficiency is obtained with the RINEPT-CWc sequence incorporating an adiabatic recoupling. This recoupling also leads to the highest robustness to offset and rf inhomogeneity, and SR4$_1^2$(tt) and R12$_3^5$(tt) yield identical transfer

390   efficiency and robustness. Hence, the three-step multiple-quantum super-cycle of the SR4$_1^2$ symmetry does not improve the robustness in the case of a tanh/tan basic element. However, these recoupling schemes require maximum rf fields of $v_{1,max} \geq 8v_R = 160$ kHz, which may exceed the rf power specifications of most 3.2 mm MAS probes.

The PRESTO sequences using R22$_2^7$(180$_0$) and R18$_2^5$(180$_0$) recoupling also result in good transfer efficiencies, *i.e.*, 27 and 39 %, respectively, but lower than RINEPT-CWc-SR4$_1^2$(tt). However, they use rf-fields of $v_1/v_R = 5.5$ and 4.5, which are

395   compatible with the specifications of 3.2 mm MAS probes. The higher transfer efficiency of R22$_2^7$(180$_0$) with respect to R18$_2^5$(180$_0$) stems from its weaker second-order cross-terms between ^{1}H-^{1}H interactions (Table 1).

The efficiency of the RINEPT-CWc-SR4$_1^2$(270$_0$90$_{180}$) sequence, with rf-field $v_1 = 4v_R$, is comparable to that of PRESTO-R18$_2^5$(180$_0$), but with a higher robustness to offset and rf inhomogeneity. We can notice that amplitude modulated recoupling schemes, for which the phase shifts are equal to 180°, such as SR4$_1^2$(270$_0$90$_{180}$) and SR4$_1^2$(180$_0$), exhibit a high robustness to

400   offset (Fig.5).(Carravetta et al., 2000) The use of 270$_0$90$_{180}$ composite pulses in SR4$_1^2$ symmetries instead of single π pulses improves their transfer efficiency as well as their robustness to offset and rf field inhomogeneity.

In summary, for $v_R = 20$ kHz in γ-alumina, the RINEPT-CWc-SR4$_1^2$(270$_0$90$_{180}$) sequence achieves efficient and robust transfers of magnetization from protons to ^{27}Al nuclei using a moderate rf field of $v_1 = 4v_R$. For ^{1}H spectra with a width smaller than 20

kHz and MAS probes with a good rf-homogeneity, PRESTO-R$22_2^7(180_0)$ sequence can result in slightly higher transfer
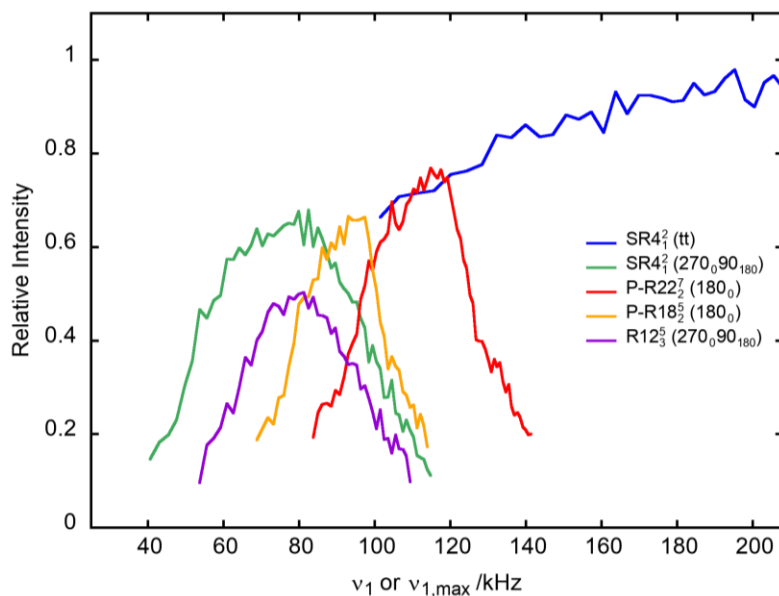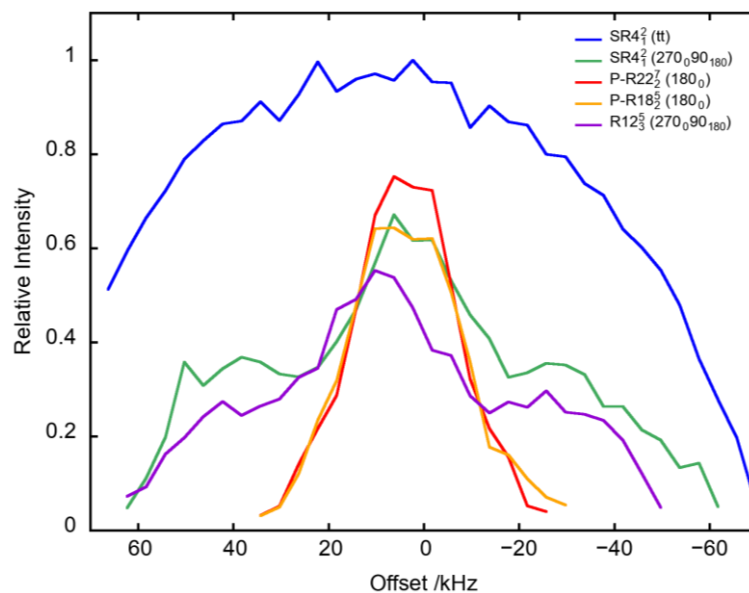
405 efficiencies.

Figure 4: Variation at ν_R = 20 kHz of the ^{27}AlO$_6$ signal of γ-alumina as function of ν_1 or $\nu_{1,max}$ of the recoupling for PRESTO-R$22_2^7(180_0)$ and -R$18_2^5(180_0)$ as well as RINEPT-SR4_1^2 (tt), -SR4_1^2 ($270_0 90_{180}$) and -R12_3^5 ($270_0 90_{180}$). For each curve τ was fixed to its optimum value given in Table 5.

410

Figure 5: Variation at ν_R = 20 kHz of the ^{27}AlO$_6$ signal of γ-alumina as function of offset of the recoupling for PRESTO-R$22_2^7(180_0)$ and -R$18_2^5(180_0)$ as well as RINEPT-SR4_1^2 (tt), -SR4_1^2 ($270_0 90_{180}$) and -R12_3^5 ($270_0 90_{180}$). For each curve τ and ν_1 or $\nu_{1,max}$ were fixed to their optimum values given in Table 5.

Table 5. Comparison of the performances of $^1H \rightarrow {}^{27}Al$ RINEPT-CWc and PRESTO transfers using various recoupling for AlO_6 signal of γ-alumina at ν_R = 20 kHz.

PRESTO /RINEPT	Recoupling	τ /μs	$\nu_1/\nu_{1,max}$ /kHz	AlO_6 [a]	$\Delta\nu_0$ [b] /kHz	$\Delta\nu_0/\nu_1$	$\Delta\nu_1$ [c] /kHz	$\Delta\nu_1/\nu_1$
RINEPT	$SR4_1^2(tt)$	400	160	1	110	0.68	> 100[d]	> 0.62
	$R12_3^5(tt)$	400	160	1	110	0.68	> 100[d]	> 0.62
PRESTO	$R22_2^7(180_0)$	400	110	0.73	30	0.27	39	0.35
RINEPT	$SR4_1^2(270_090_{180})$	400	80	0.63	50	0.63	44	0.55
PRESTO	$R18_2^5(180_0)$	400	90	0.61	28	0.31	27	0.30
RINEPT	$R12_3^5(270_090_{180})$	400	80	0.50	40	0.50	35	0.44
	$SR4_1^2(90_{-45}90_{45}90_{-45})$	400	63	0.42	14	0.22	14	0.22
	$SR4_1^2(180_0)$	400	45	0.40	17	0.38	24	0.53
	$R12_3^5(180_0)$	400	45	0.35	10	0.22	15	0.33
	$R12_3^5(90_{-45}90_{45}90_{-45})$	400	66	0.35	11	0.17	18	0.27
	$SC2_1^0$	400	63	0.31	14	0.22	45	0.71
	$C6_3^0$	400	66	0.28	10	0.15	40	0.60

[a] AlO_6 signal normalized to that with $^1H \rightarrow {}^{27}Al$ RINEPT-CWc-$SR4_1^2(tt)$. [b] FWHM of the robustness to offset. [c] FWHM of the robustness to rf-field. [d] Only a lower bound of rf-field could be determined due to probe rf specifications (Fig.4).

IV-3-2. Isopropylamine-templated $AlPO_4$-14

Fig.6 shows the 1D $^1H \rightarrow {}^{27}Al$ RINEPT and PRESTO spectra of $AlPO_4$-14. They exhibits three ^{27}Al resonances at 43, 21 and −2 ppm assigned to AlO_4, AlO_5 and AlO_6 sites, respectively.(Ashbrook et al., 2008) The AlO_5 and AlO_6 sites are directly bonded to OH groups. The ^1H MAS spectrum is shown in Fig.S1. According to the literature, the $^{27}AlO_4$ signal subsumes the resonances of two AlO_4 sites with quadrupolar coupling constants C_Q = 1.7 and 4.1 MHz, whereas the C_Q constants of $^{27}AlO_5$ and $^{27}AlO_6$ sites are equal to 5.6 and 2.6 MHz, respectively.(Fernandez et al., 1996; Antonijevic et al., 2006) The ^1H-^1H dipolar couplings within the isopropylamine template molecule are larger than in γ-alumina. We used the most intense peak, AlO_4, to compare the $^1H \rightarrow {}^{27}Al$ transfer efficiencies of RINEPT-CWc and PRESTO sequences with different recoupling schemes, and the results are given in Table 6. The six sequences yielding the highest transfer efficiencies are the same for $AlPO_4$-14 and γ-alumina and their relative efficiencies are comparable for the AlO_4 peak of $AlPO_4$-14 and the AlO_6 signal of γ-alumina.
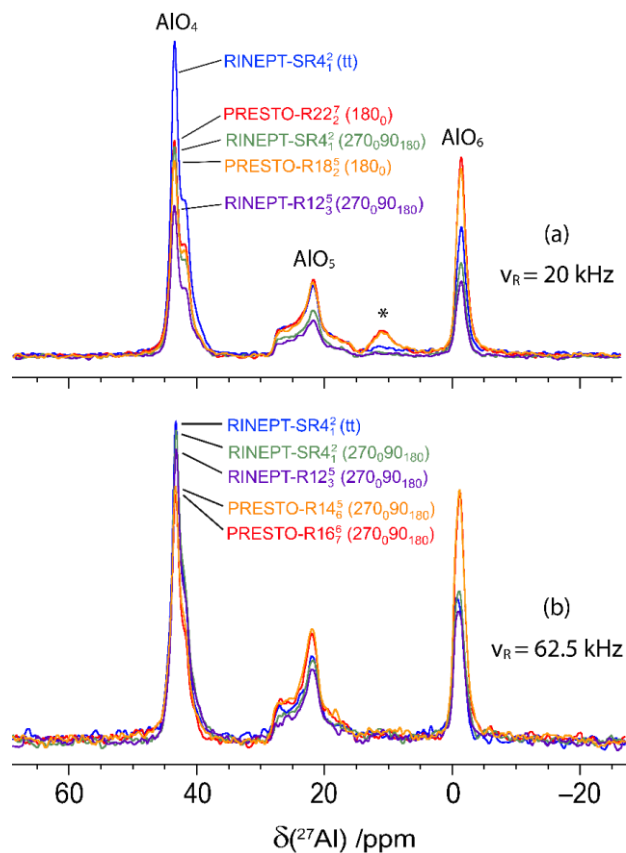
Figure 6: 1D ^{27}Al spectra of AlPO$_4$-14 at B$_0$ = 18.8 T with ν_R = 20 (a) and 62.5 (b) kHz acquired using ^{1}H → ^{27}Al RINEPT-CWc and PRESTO-III transfers using the following recoupling schemes: SR4$_1^2$(tt), SR4$_1^2$(270$_0$90$_{180}$) and R12$_3^5$(270$_0$90$_{180}$) for RINEPT, and (a) R22$_2^7$(180$_0$) and R18$_2^5$ (180$_0$), or (b) R16$_7^6$ (270$_0$90$_{180}$) and R14$_6^5$ (270$_0$90$_{180}$) for PRESTO. τ delay and $\nu_1/\nu_{1,max}$ rf field were fixed to their optimal values given in Tables 6 and 8. The resonance at $ca.$ 11 ppm in (a) is due to an impurity.

Nevertheless, the rf requirement of the SR4$_1^2$(tt) and R12$_3^5$(tt) schemes is higher for AlPO$_4$-14 than for γ-alumina because of larger ^{1}H-^{1}H dipolar couplings, in agreement with the numerical simulations of Figs.2a-c. This rf requirement prevents the use of these adiabatic recoupling schemes at ν_R = 20 kHz with most 3.2 mm MAS probes. The rf requirement of the other sequences, and their robustness to offset and rf-fields homogeneity are similar for both samples (Table 6 and Figs.S2 and S3). With respect to the RINEPT sequence, PRESTO yields higher transfer efficiency for AlO$_5$ and AlO$_6$ resonances than for AlO$_4$ signals in the case of AlPO$_4$-14 since (i) these Al sites are directly bonded to OH groups and (ii) R22$_2^7$(180$_0$) and R18$_2^5$(180$_0$) recoupling schemes are subject to dipolar truncation (section II-1-1), which prevents to transfer the ^{1}H magnetization of these OH groups to ^{27}AlO$_4$ nuclei.

Hence, for both AlPO$_4$-14 and γ-alumina, RINEPT-CWc-SR4$_1^2$(270$_0$90$_{180}$) and PRESTO-R22$_2^7$(180$_0$) sequences are the methods of choice to transfer ^{1}H magnetization to ^{27}Al nuclei at ν_R = 20 kHz.

Table 6. Comparison of the performances of $^1H \rightarrow {}^{27}Al$ RINEPT-CWc and PRESTO transfers with $AlPO_4$-14 at ν_R = 20 kHz.

PRESTO /RINEPT	Recoupling	τ /μs	$\nu_1/\nu_{1,max}$ /kHz	Intensity [a]			$\Delta\nu_0$ /kHz	$\Delta\nu_0/\nu_1$	$\Delta\nu_1$ /kHz	$\Delta\nu_1/\nu_1$
				AlO_6	AlO_5	AlO_4				
RINEPT	$SR4^2_1(tt)$	800	208	1	1	1	120	0.58	-[b]	-[b]
	$R12^5_3(tt)$	800	208	0.99	0.99	0.98	120	0.58	-[b]	-[b]
PRESTO	$R22^7_2(180_0)$	600	114	1.54	1.07	0.67	26	0.23	38	0.33
RINEPT	$SR4^2_1(270_090_{180})$	800	77	0.72	0.65	0.67	45	0.58	48	0.62
PRESTO	$R18^5_2(180_0)$	600	94	1.45	1.03	0.62	25	0.27	26	0.28
RINEPT	$R12^5_3(270_090_{180})$	800	77	0.58	0.50	0.48	46	0.60	36	0.47
	$SR4^2_1(180_0)$	600	43	0.64	0.45	0.36	14	0.33	23	0.53
	$SR4^2_1(90_{-45}90_{45}90_{-45})$	800	61	0.56	0.43	0.25	16	0.26	20	0.32
	$SC2^0_1$	800	68	0.54	0.41	0.24	18	0.26	52	0.73
	$R12^5_3(90_{-45}90_{45}90_{-45})$	600	61	0.43	0.30	0.21	8	0.13	18	0.29
	$R12^5_3(180_0)$	600	45	0.34	0.28	0.21	8	0.18	18	0.40
	$C6^0_3$	600	68	0.52	0.36	0.21	10	0.15	42	0.61

[a] Intensities of AlO_6, AlO_5 and AlO_4 resonances normalized to their intensities with $^1H \rightarrow {}^{27}Al$ RINEPT-CWc-$SR4^2_1(tt)$.
[b] FWHM of the robustness to rf-field was not measured for RINEPT-$SR4^2_1(tt)$ and -$R12^5_3(tt)$ (Fig.S1).

450

IV-4. PRESTO and RINEPT performances for ν_R = 62.5 kHz

Similar comparisons of the performances of the various RINEPT-CWc and PRESTO sequences were performed for γ-alumina and $AlPO_4$-14 at ν_R = 62.5 kHz.

IV-4-1. γ-alumina

455   The corresponding data for γ-alumina are given Table 7. The sequences yielding the highest transfer efficiencies are by decreasing order RINEPT-CWc with $SR4^2_1(tt)$ or $R12^5_3(tt)$ > RINEPT-CWc-$SR4^2_1(270_090_{180})$ ≈ PRESTO-$R16^6_7(270_090_{180})$ > PRESTO-$R14^5_6(270_090_{180})$ > RINEPT-CWc-$R12^5_3(270_090_{180})$.

Nevertheless, the nominal rf requirements of the RINEPT sequences using adiabatic pulses or 270_090_{180} composite π-pulses correspond to ν_{1max} = $5\nu_R$ (313 kHz: Fig.2d) or $4\nu_R$ (250 kHz), which exceeds the specifications of our 1.3 MAS probe, and the

460 sequences were tested only up to ν_{1max} = 208 kHz (Fig.7). This suboptimal rf field could potentially limit the transfer efficiencies of these sequences.

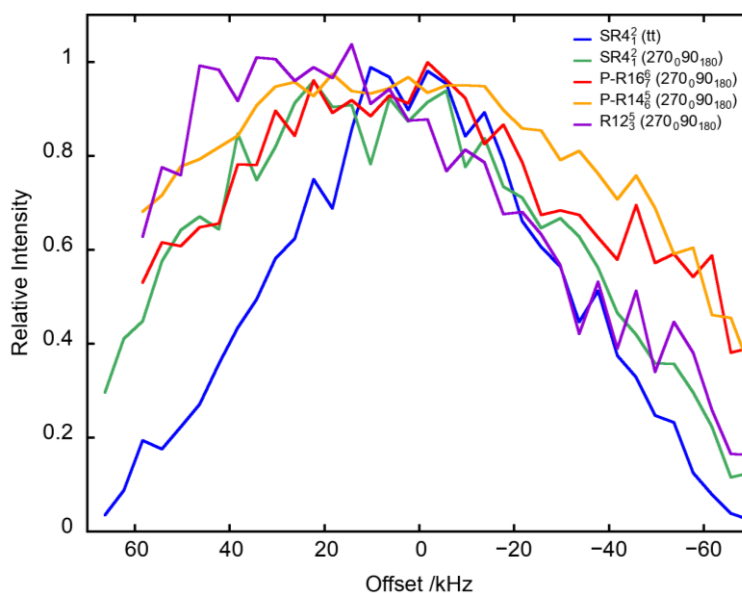The PRESTO-$R16^6_7(270_090_{180})$ and -$R14^5_6(270_090_{180})$ sequences yield transfer efficiencies comparable to those of RINEPT-CWc-$SR4^2_1(270_090_{180})$, but with a significantly lower rf field, 137 kHz ≈ $2.3\nu_R$. Furthermore, the robustness to offset of these

PRESTO sequences is comparable to that of RINEPT-CWc-SR4$_1^2$(270$_0$90$_{180}$) (Fig.8). PRESTO-R22$_4^3$(180$_0$) and -R16$_3^2$(180$_0$)

465   sequences with the small phase shift of $2\phi \leq 52°$ are less efficient because they are sensitive to rf inhomogeneity.
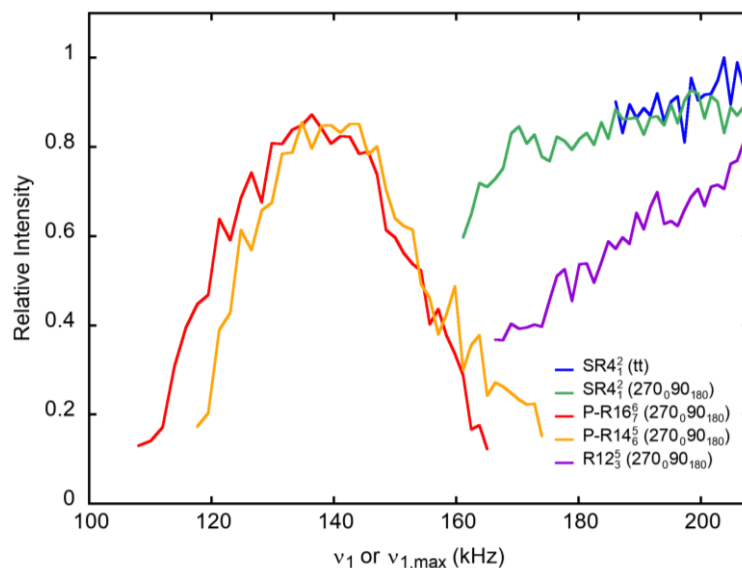
Figure 7: Variation at ν_R = 62.5 kHz of the ^{27}AlO$_6$ signal of γ-alumina as function of ν_1 or $\nu_{1,max}$ of the recoupling for PRESTO-R16$_7^6$(270$_0$90$_{180}$) and -R14$_6^5$(270$_0$90$_{180}$) as well as RINEPT-SR4$_1^2$ (tt), -SR4$_1^2$ (270$_0$90$_{180}$) and -R12$_3^5$ (270$_0$90$_{180}$). For each curve τ was
470   **fixed to its optimum value given in Table 7.**

Figure 8: Variation at ν_R = 62.5 kHz of the ^{27}AlO$_6$ signal of γ-alumina as function of offset of the recoupling for PRESTO-R16$_7^6$(270$_0$90$_{180}$) and -R14$_6^5$(270$_0$90$_{180}$) as well as RINEPT-SR4$_1^2$ (tt), -SR4$_1^2$ (270$_0$90$_{180}$) and -R12$_3^5$ (270$_0$90$_{180}$). For each curve τ and ν_1 or $\nu_{1,max}$ were fixed to their optimum values given in Table 7.

475 **Table 7. Comparison of the performances of $^1H \rightarrow ^{27}Al$ RINEPT-CWc and PRESTO transfer using various recoupling for the AlO$_6$ signal of γ-alumina at ν_R = 62.5 kHz.**

PRESTO/RINEPT	Recoupling	τ /μs	$\nu_1/\nu_{1,max}$ /kHz	AlO$_6$ [a]	$\Delta\nu_0$ /kHz	$\Delta\nu_0/\nu_1$	$\Delta\nu_1$ /kHz	$\Delta\nu_1/\nu_1$
	$SR4_1^2(tt)$	256	208	1	74	0.36	-[b]	-[b]
RINEPT	$R12_3^5(tt)$	256	208	1	74	0.36	-[b]	-[b]
	$SR4_1^2(270_090_{180})$	320	208	0.92	96	0.46	-[b]	-[b]
PRESTO	$R16_7^6(270_090_{180})$	448	137	0.91	90	0.66	42	0.31
	$R14_6^5(270_090_{180})$	384	146	0.86	100	0.68	38	0.26
	$R12_3^5(270_090_{180})$	320	208	0.82	86	0.41	-[b]	-[b]
RINEPT	$SR4_1^2(180_0)$	320	125	0.75	52	0.42	88	0.70
	$R12_3^5(180_0)$	288	125	0.74	16	0.13	85	0.68
PRESTO	$R22_4^3(180_0)$	256	157	0.67	68	0.43	20	0.13
	$R16_3^2(180_0)$	384	155	0.51	48	0.31	40	0.26
	$SC2_1^0$	256	186	0.34	50	0.27	84	0.45
RINEPT	$C6_3^0$	256	186	0.34	43	0.23	76	0.41
	$SR4_1^2(90_{-45}90_{45}90_{-45})$	256	186	0.32	47	0.25	70	0.38
	$R12_3^5(90_{-45}90_{45}90_{-45})$	256	186	0.32	40	0.22	70	0.38

[a] Intensities of AlO$_6$, AlO$_5$ and AlO$_4$ resonances normalized to their intensities with $^1H \rightarrow ^{27}Al$ RINEPT-CWc-$SR4_1^2(tt)$.
[b] FWHM of the robustness to rf-field was not measured for RINEPT-$SR4_1^2(tt)$ and -$R12_3^5(tt)$ (Fig.7).

505 **IV-4-2. Isopropylamine-templated AlPO$_4$-14**

In the case of AlPO$_4$-14, the relative transfer efficiencies for $^{27}AlO_4$ nuclei follow a similar order as for γ-alumina, except that the transfer efficiencies of PRESTO-$R16_7^6(270_090_{180})$ and -$R14_6^5(270_090_{180})$ are significantly lower than that of RINEPT-CWc-$SR4_1^2(270_090_{180})$ (Table 8). This decreased efficiency of the PRESTO schemes for AlO$_4$ stems notably from the dipolar truncation, which prevents the transfer of magnetization from the protons of OH groups bonded to AlO$_5$ and AlO$_6$ sites to

510 $^{27}AlO_4$ nuclei. In Table. S1 we give the ^1H-^{27}Al distances of AlPO$_4$-14, which confirms that OH groups are closer to AlO$_5$ and AlO$_6$ sites, and hence, why the transfer efficiency for PRESTO-$R16_7^6(270_090_{180})$ and -$R14_6^5(270_090_{180})$ is higher than for RINEPT-CWc-$SR4_1^2(270_090_{180})$. However, the latter sequence uses amplitude-modulated recoupling, and hence benefits from a higher robustness to rf-field inhomogeneity than the PRESTO schemes (Fig.S3). Conversely, the robustness to offset of these three sequences are comparable (Fig.S4), whereas the rf requirements of $R16_7^6(270_090_{180})$ and $R14_6^5(270_090_{180})$ are much lower

515 than that of $SR4_1^2(270_090_{180})$.

In summary, at ν_R = 62.5 kHz, for both γ-alumina and isopropylamine-templated AlPO$_4$-14, PRESTO-R16$_7^6$(270$_0$90$_{180}$) and RINEPT-CWc-SR4$_1^2$(270$_0$90$_{180}$) are the methods of choice to transfer polarization of protons to quadrupolar nuclei. However, the first sequence requires a much lower rf-field than the second.

Table 8. Comparison of the performances of ^{1}H $\rightarrow$ ^{27}Al RINEPT-CWc and PRESTO transfers using various recoupling for AlPO$_4$-14 at ν_R = 62.5 kHz.

PRESTO /RINEPT	Recoupling	τ /μs	$\nu_1/\nu_{1,max}$ /kHz	Intensity [a]			$\Delta\nu_0$ /kHz	$\Delta\nu_0/\nu_1$	$\Delta\nu_1$ /kHz	$\Delta\nu_1/\nu_1$
				AlO$_6$	AlO$_5$	AlO$_4$				
RINEPT	SR4$_1^2$(tt)	480	208	1	1	1	48	0.23	-[b]	-[b]
	R12$_3^5$(tt)	480	208	1.07	1	1.06	44	0.21	-[b]	-[b]
	SR4$_1^2$(270$_0$90$_{180}$)	480	208	1.05	0.95	0.97	85	0.41	90	0.43
	R12$_3^5$(270$_0$90$_{180}$)	480	208	0.91	0.84	0.91	80	0.38	68	0.33
PRESTO	R16$_7^6$(270$_0$90$_{180}$)	672	146	1.71	1.21	0.76	80	0.55	50	0.34
	R14$_6^5$(270$_0$90$_{180}$)	576	146	1.72	1.27	0.76	86	0.59	45	0.31
RINEPT	SR4$_1^2$(180$_0$)	480	129	0.84	0.79	0.75	48	0.37	64	0.49
	R12$_3^5$(180$_0$)	480	136	0.72	0.67	0.74	18	0.13	54	0.40
PRESTO	R22$_4^3$(180$_0$)	512	157	1.47	1.18	0.69	60	0.38	20	0.33
	R16$_3^2$(180$_0$)	480	147	1.17	0.83	0.52	64	0.44	20	0.31
RINEPT	R12$_3^5$(90$_{-45}$90$_{45}$90$_{-45}$)	256	190	0.48	0.27	0.14	32	0.17	75	0.39
	C6$_3^0$(C')	256	193	0.47	0.28	0.14	28	0.15	78	0.40
	SR4$_1^2$(90$_{-45}$90$_{45}$90$_{-45}$)	256	196	0.48	0.14	0.14	36	0.18	77	0.39
	SC2$_1^0$(C)	256	188	0.53	0.25	0.14	44	0,23	80	0.43

[a] Intensities of AlO$_6$, AlO$_5$ and AlO$_4$ resonances normalized to their intensities with ^{1}H$\rightarrow$^{27}Al RINEPT-CWc-SR4$_1^2$(tt).
[b] FWHM of the robustness to rf-field was not measured for RINEPT-SR4$_1^2$(tt) and -R12$_3^5$(tt) (Fig.S3).

V. Conclusions

In this work, we have introduced novel symmetry-based hetero-nuclear dipolar recoupling schemes, which can be incorporated into the RINEPT and PRESTO sequences to transfer the magnetization from protons to half-integer quadrupolar nuclei at ν_R = 20 or 62.5 kHz. These novel recouplings have been compared to existing schemes. We have shown that the RINEPT-CWc-SR4$_1^2$(tt) sequence, which produces efficient and robust transfers at ν_R $\approx$ 10-15 kHz,(Nagashima et al., 2020) requires rf-fields incompatible with the specifications of most MAS probes for ν_R $\geq$ 20 kHz. Conversely, the introduced RINEPT-CWc-SR4$_1^2$(270$_0$90$_{180}$) and PRESTO-R22$_2^7$(180$_0$) techniques with rf-fields of 4ν_R and 5.5ν_R, respectively, are the methods of choice

at ν_R = 20 kHz to transfer the magnetization from protons to quadrupolar nuclei. At ν_R = 62.5 kHz, the RINEPT-CWc-SR4$_1^2$(270$_0$90$_{180}$) and PRESTO-R16$_7^6$(270$_0$90$_{180}$) sequences with rf-requirements of 4ν_R and 2.3ν_R, respectively, result in the most robust and efficient transfers. At both MAS frequencies, the RINEPT and PRESTO techniques complement each other since the latter is dipolar truncated, whereas the former is not. As result, the RINEPT sequences must be chosen to observe

535 simultaneously protonated and unprotonated sites, whereas the PRESTO schemes can be employed for the selective observation of quadrupolar nuclei in proximity to protons. These techniques are expected to be useful for transferring the DNP-enhanced magnetization of protons to quadrupolar nuclei in indirect MAS DNP experiments at $\nu_R \geq 20$ kHz, notably used at high magnetic fields.(Nagashima et al., 2020, n.d.; Rankin et al., 2019; Berruyer et al., 2020)

540 **Author contributions**: JSG, AGMR and JT carried out the NMR experiments on γ-alumina and AlPO$_4$-14. YT performed the spin dynamics simulations and carried out the NMR experiments on l-histidine·HCl. OL derived average Hamiltonian theory for the investigated recoupling sequences. OL and JPA wrote the manuscript. All the authors contributed to the editing of the manuscript.

Acknowledgments

References

Amoureux, J.-P. and Pruski, M.: Theoretical and experimental assessment of single- and multiple-quantum cross-polarization in solid state NMR, 100, 1595–1613, https://doi.org/10.1080/00268970210125755, 2002.

555 Antonijevic, S., Ashbrook, S. E., Biedasek, S., Walton, R. I., Wimperis, S., and Yang, H.: Dynamics on the Microsecond Timescale in Microporous Aluminophosphate AlPO-14 as Evidenced by 27Al MQMAS and STMAS NMR Spectroscopy, J. Am. Chem. Soc., 128, 8054–8062, https://doi.org/10.1021/ja057682g, 2006.

Ashbrook, S. E. and Sneddon, S.: New Methods and Applications in Solid-State NMR Spectroscopy of Quadrupolar Nuclei, J. Am. Chem. Soc., 136, 15440–15456, https://doi.org/10.1021/ja504734p, 2014.

560   Ashbrook, S. E. and Wimperis, S.: Spin-locking of half-integer quadrupolar nuclei in nuclear magnetic resonance of solids: Second-order quadrupolar and resonance offset effects, J. Chem. Phys., 131, 194509, https://doi.org/10.1063/1.3263904, 2009.

Ashbrook, S. E., Cutajar, M., Pickard, C. J., Walton, R. I., and Wimperis, S.: Structure and NMR assignment in calcined and as-synthesized forms of AlPO-14: a combined study by first-principles calculations and high-resolution 27Al–31P MAS NMR correlation, Phys. Chem. Chem. Phys., 10, 5754–5764, https://doi.org/10.1039/B805681A, 2008.

565   Bak, M. and Nielsen, N. C.: REPULSION, A Novel Approach to Efficient Powder Averaging in Solid-State NMR, Journal of Magnetic Resonance, 125, 132–139, https://doi.org/10.1006/jmre.1996.1087, 1997a.

Bak, M., Rasmussen, J. T., and Nielsen, N. C.: SIMPSON: a general simulation program for solid-state NMR spectroscopy., 147, 296–330, https://doi.org/10.1006/jmre.2000.2179, 2000.

Barrie, P. J.: Distorted powder lineshapes in ^{27}Al CP / MAS NMR spectroscopy of solids, Chemical Physics Letters, 208,
570   486–490, https://doi.org/10.1016/0009-2614(93)87177-5, 1993.

Berruyer, P., Björgvinsdóttir, S., Bertarello, A., Stevanato, G., Rao, Y., Karthikeyan, G., Casano, G., Ouari, O., Lelli, M., Reiter, C., Engelke, F., and Emsley, L.: Dynamic Nuclear Polarization Enhancement of 200 at 21.15 T Enabled by 65 kHz Magic Angle Spinning, J. Phys. Chem. Lett., 11, 8386–8391, https://doi.org/10.1021/acs.jpclett.0c02493, 2020.

Blanc, F., Sperrin, L., Jefferson, D. A., Pawsey, S., Rosay, M., and Grey, C. P.: Dynamic Nuclear Polarization Enhanced
575   Natural Abundance ^{17}O Spectroscopy, J. Am. Chem. Soc., 135, 2975–2978, https://doi.org/10.1021/ja4004377, 2013.

Brinkmann, A. and Edén, M.: Second order average Hamiltonian theory of symmetry-based pulse schemes in the nuclear magnetic resonance of rotating solids: Application to triple-quantum dipolar recoupling, 120, 11726, https://doi.org/10.1063/1.1738102, 2004b.

Brinkmann, A. and Kentgens, A. P. M.: Proton-Selective ^{17}O−^{1}H Distance Measurements in Fast Magic-Angle-Spinning
580   Solid-State NMR Spectroscopy for the Determination of Hydrogen Bond Lengths, J. Am. Chem. Soc., 128, 14758–14759, https://doi.org/10.1021/ja065415k, 2006a.

Brinkmann, A. and Kentgens, A. P. M.: Sensitivity Enhancement and Heteronuclear Distance Measurements in Biological ^{17}O Solid-State NMR, J. Phys. Chem. B, 110, 16089–16101, https://doi.org/10.1021/jp062809p, 2006b.

Brinkmann, A. and Levitt, M. H.: Symmetry principles in the nuclear magnetic resonance of spinning solids: Heteronuclear
585   recoupling by generalized Hartmann-Hahn sequences, 115, 357–384, https://doi.org/10.1063/1.1377031, 2001.

Brinkmann, A., Edén, M., and Levitt, M. H.: Synchronous helical pulse sequences in magic-angle spinning nuclear magnetic resonance: double quantum recoupling of multiple-spin systems, 112, 8539–8554, https://doi.org/10.1063/1.481458, 2000.

Carravetta, M., Edén, M., Zhao, X., Brinkmann, A., and Levitt, M. H.: Symmetry principles for the design of radiofrequency pulse sequences in the nuclear magnetic resonance of rotating solids, Chemical Physics Letters, 321, 205–215,
590   https://doi.org/10.1016/S0009-2614(00)00340-7, 2000.

Chen, J., Wu, X.-P., Hope, M. A., Qian, K., Halat, D. M., Liu, T., Li, Y., Shen, L., Ke, X., Wen, Y., Du, J.-H., Magusin, P. C. M. M., Paul, S., Ding, W., Gong, X.-Q., Grey, C. P., and Peng, L.: Polar surface structure of oxide nanocrystals revealed with solid-state NMR spectroscopy, Nat Commun, 10, 1–10, https://doi.org/10.1038/s41467-019-13424-7, 2019.

MAGNETIC
RESONANCE
Open Access
Discussions

595   Ding, S. W. and Mcdowell, C. A.: Theoretical Calculations of the CPMAS Spectral Lineshapes of Half-Integer Quadrupole Systems, Journal of Magnetic Resonance, Series A, 114, 80–87, https://doi.org/10.1006/jmra.1995.1108, 1995.

Duong, N. T., Trébosc, J., Lafon, O., and Amoureux, J.-P.: Improved sensitivity and quantification for 29Si NMR experiments on solids using UDEFT (Uniform Driven Equilibrium Fourier Transform), Solid State Nuclear Magnetic Resonance, 100, 52–62, https://doi.org/10.1016/j.ssnmr.2019.03.007, 2019.

Fernandez, C., Amoureux, J. P., Chezeau, J. M., Delmotte, L., and Kessler, H.: 27Al MAS NMR characterization of AlPO$_4$-14 enhanced resolution and information by MQMAS Dr. Hellmut G. Karge on the occasion of his 65th birthday, Microporous Materials, 6, 331–340, https://doi.org/10.1016/0927-6513(96)00040-5, 1996.

Freeman, R., Kempsell, S. P., and Levitt, M. H.: Radiofrequency pulse sequences which compensate their own imperfections, Journal of Magnetic Resonance (1969), 38, 453–479, https://doi.org/10.1016/0022-2364(80)90327-3, 1980.

Gansmüller, A., Simorre, J.-P., and Hediger, S.: Windowed R-PDLF recoupling: A flexible and reliable tool to characterize
605   molecular dynamics, Journal of Magnetic Resonance, 234, 154–164, https://doi.org/10.1016/j.jmr.2013.06.017, 2013.

Garwood, M. and DelaBarre, L.: The Return of the Frequency Sweep: Designing Adiabatic Pulses for Contemporary NMR, Journal of Magnetic Resonance, 153, 155–177, https://doi.org/10.1006/jmre.2001.2340, 2001.

Giovine, R., Trébosc, J., Pourpoint, F., Lafon, O., and Amoureux, J.-P.: Magnetization transfer from protons to quadrupolar nuclei in solid-state NMR using PRESTO or dipolar-mediated refocused INEPT methods, Journal of Magnetic Resonance,
610   299, 109–123, https://doi.org/10.1016/j.jmr.2018.12.016, 2019.

Harris, R. K. and Nesbitt, G. J.: Cross polarization for quadrupolar nuclei—Proton to sodium-23, Journal of Magnetic Resonance (1969), 78, 245–256, https://doi.org/10.1016/0022-2364(88)90268-5, 1988.

Hayashi, S. and Hayamizu, K.: Line shapes in CP/MAS NMR spectra of half-integer quadrupolar nuclei, Chemical Physics Letters, 203, 319–324, https://doi.org/10.1016/0009-2614(93)85575-9, 1993.

615   Hope, M. A., Halat, D. M., Magusin, P. C. M. M., Paul, S., Peng, L., and Grey, C. P.: Surface-selective direct ^{17}O DNP NMR of CeO$_2$ nanoparticles, Chem. Commun., 53, 2142–2145, https://doi.org/10.1039/C6CC10145C, 2017.

Hu, B., Delevoye, L., Lafon, O., Trébosc, J., and Amoureux, J. P.: Double-quantum NMR spectroscopy of 31P species submitted to very large CSAs., 200, 178–88, https://doi.org/10.1016/j.jmr.2009.06.020, 2009.

Hwang, S.-J., Chen, C.-Y., and Zones, S. I.: Boron Sites in Borosilicate Zeolites at Various Stages of Hydration Studied by
620   Solid State NMR Spectroscopy, J. Phys. Chem. B, 108, 18535–18546, https://doi.org/10.1021/jp0476904, 2004.

Kervern, G., Pintacuda, G., and Emsley, L.: Fast adiabatic pulses for solid-state NMR of paramagnetic systems, 435, 157–162, https://doi.org/10.1016/j.cplett.2006.12.056, 2007.

Lee, D., Duong, N. T., Lafon, O., and De Paëpe, G.: Primostrato Solid-State NMR Enhanced by Dynamic Nuclear Polarization: Pentacoordinated Al^{3+} Ions Are Only Located at the Surface of Hydrated γ-Alumina, 118, 25065−25076,
625   https://doi.org/10.1021/jp508009x, 2014.

MAGNETIC RESONANCE
Open Access
Discussions

Lee, D., Leroy, C., Crevant, C., Bonhomme-Coury, L., Babonneau, F., Laurencin, D., Bonhomme, C., and Paëpe, G. D.: Interfacial Ca^{2+} environments in nanocrystalline apatites revealed by dynamic nuclear polarization enhanced ^{43}Ca NMR spectroscopy, 8, 14104, https://doi.org/10.1038/ncomms14104, 2017.

Levitt, M. H.: Symmetry-based pulse sequences in magic-angle spinning solid-state NMR, in: Encyclopedia of Nuclear

630   Magnetic Resonance. Volume 9, Advances in NMR, edited by: Grant, D. M. and Harris, R. K., Wiley, 165–196, 2002.

Levitt, M. H. and Freeman, R.: NMR population inversion using a composite pulse, 33, 473–476, https://doi.org/10.1016/0022-2364(79)90265-8, 1979.

Li, W., Wang, Q., Xu, J., Aussenac, F., Qi, G., Zhao, X., Gao, P., Wang, C., and Deng, F.: Probing the surface of γ-Al_2O_3 by oxygen-17 dynamic nuclear polarization enhanced solid-state NMR spectroscopy, Phys. Chem. Chem. Phys., 20, 17218–

635   17225, https://doi.org/10.1039/C8CP03132K, 2018.

Liang, L., Hou, G., and Bao, X.: Measurement of proton chemical shift anisotropy in solid-state NMR spectroscopy, Solid State Nuclear Magnetic Resonance, 93, 16–28, https://doi.org/10.1016/j.ssnmr.2018.04.002, 2018.

Lu, X., Lafon, O., Trébosc, J., Tricot, G., Delevoye, L., Méar, F., Montagne, L., and Amoureux, J. P.: Observation of proximities between spin-1/2 and quadrupolar nuclei: which heteronuclear dipolar recoupling method is preferable?, 137,

640   144201, https://doi.org/10.1063/1.4753987, 2012.

Madhu, P. K., Zhao, X., and Levitt, M. H.: High-resolution ^1H NMR in the solid state using symmetry-based pulse sequences, 346, 142–148, https://doi.org/10.1016/S0009-2614(01)00876-4, 2001.

Martineau, C., Bouchevreau, B., Taulelle, F., Trébosc, J., Lafon, O., and Amoureux, J. P.: High-resolution through-space correlations between spin-1/2 and half-integer quadrupolar nuclei using the MQ-D-R-INEPT NMR experiment, Phys. Chem.

645   Chem. Phys., 14, 7112–7119, https://doi.org/10.1039/C2CP40344G, 2012.

Morris, H. D. and Ellis, P. D.: Aluminum-27 cross polarization of aluminas. The NMR spectroscopy of surface aluminum atoms, J. Am. Chem. Soc., 111, 6045–6049, https://doi.org/10.1021/ja00198a012, 1989.

Nagashima, H., Lilly Thankamony, A. S., Trébosc, J., Montagne, L., Kerven, G., Amoureux, J.-P., and Lafon, O.: Observation of proximities between spin-1/2 and quadrupolar nuclei in solids: Improved robustness to chemical shielding using adiabatic

650   symmetry-based recoupling, Solid State Nuclear Magnetic Resonance, 94, 7–19, https://doi.org/10.1016/j.ssnmr.2018.07.001, 2018.

Nagashima, H., Trébosc, J., Kon, Y., Sato, K., Lafon, O., and Amoureux, J.-P.: Observation of Low-γ Quadrupolar Nuclei by Surface-Enhanced NMR Spectroscopy, J. Am. Chem. Soc., 142, 10659–10672, https://doi.org/10.1021/jacs.9b13838, 2020.

Nagashima, H., Trebosc, J., Kon, Y., Lafon, O., and Amoureux, J.-P.: Efficient transfer of ^1H magnetization to half-integer

655   quadrupolar nuclei in solids, enhanced by dynamic nuclear polarization at moderate spinning rate, Magnetic Resonance in Chemistry, In press, https://doi.org/10.1002/mrc.5121, n.d.

Pandey, M. K., Malon, M., Ramamoorthy, A., and Nishiyama, Y.: Composite-180° pulse-based symmetry sequences to recouple proton chemical shift anisotropy tensors under ultrafast MAS solid-state NMR spectroscopy, Journal of Magnetic Resonance, 250, 45–54, https://doi.org/10.1016/j.jmr.2014.11.002, 2015.

660 Peng, L., Huo, H., Liu, Y., and Grey, C. P.: ^{17}O Magic Angle Spinning NMR Studies of Brønsted Acid Sites in Zeolites HY and HZSM-5, J. Am. Chem. Soc., 129, 335–346, https://doi.org/10.1021/ja064922z, 2007.

Perras, F. A., Kobayashi, T., and Pruski, M.: Natural Abundance [17]O DNP Two-Dimensional and Surface-Enhanced NMR Spectroscopy, J. Am. Chem. Soc., 137, 8336–8339, https://doi.org/10.1021/jacs.5b03905, 2015a.

Perras, F. A., Kobayashi, T., and Pruski, M.: PRESTO polarization transfer to quadrupolar nuclei: implications for dynamic
665 nuclear polarization, Phys. Chem. Chem. Phys., 17, 22616–22622, https://doi.org/10.1039/C5CP04145G, 2015b.

Perras, F. A., Chaudhary, U., Slowing, I. I., and Pruski, M.: Probing Surface Hydrogen Bonding and Dynamics by Natural Abundance, Multidimensional, ^{17}O DNP-NMR Spectroscopy, J. Phys. Chem. C, 120, 11535–11544, https://doi.org/10.1021/acs.jpcc.6b02579, 2016.

Perras, F. A., Wang, Z., Naik, P., Slowing, I. I., and Pruski, M.: Natural Abundance ^{17}O DNP NMR Provides Precise O−H
670 Distances and Insights into the Brønsted Acidity of Heterogeneous Catalysts, Angewandte Chemie International Edition, 56, 9165–9169, https://doi.org/10.1002/anie.201704032, 2017.

Perras, F. A., Goh, T. W., Wang, L.-L., Huang, W., and Pruski, M.: Enhanced 1H-X D-HMQC performance through improved 1H homonuclear decoupling, Solid State Nuclear Magnetic Resonance, 98, 12–18, https://doi.org/10.1016/j.ssnmr.2019.01.001, 2019.

675 Pileio, G., Concistrè, M., McLean, N., Gansmüller, A., Brown, R. C. D., and Levitt, M. H.: Analytical theory of γ-encoded double-quantum recoupling sequences in solid-state nuclear magnetic resonance, Journal of Magnetic Resonance, 186, 65–74, https://doi.org/10.1016/j.jmr.2007.01.009, 2007.

Rankin, A. G. M., Trébosc, J., Pourpoint, F., Amoureux, J.-P., and Lafon, O.: Recent developments in MAS DNP-NMR of materials, Solid State Nuclear Magnetic Resonance, 101, 116–143, https://doi.org/10.1016/j.ssnmr.2019.05.009, 2019.

680 Rocha, J., Carr, S. W., and Klinowski, J.: [27]Al quadrupole nutation and [1]H-[27]Al cross-polarization solid-state NMR studies of ultrastable zeolite Y with fast magic-angle spinning, Chemical Physics Letters, 187, 401–408, https://doi.org/10.1016/0009-2614(91)80272-Y, 1991.

Tricot, G., Lafon, O., Trébosc, J., Delevoye, L., Méar, F., Montagne, L., and Amoureux, J.-P.: Structural characterisation of phosphate materials: new insights into the spatial proximities between phosphorus and quadrupolar nuclei using the D-HMQC
685 MAS NMR technique, Phys. Chem. Chem. Phys., 13, 16786–16794, https://doi.org/10.1039/C1CP20993K, 2011.

Vega, A. J.: CPMAS of quadrupolar $S = 32$ nuclei, Solid State Nuclear Magnetic Resonance, 1, 17–32, https://doi.org/10.1016/0926-2040(92)90006-U, 1992.

Vitzthum, V., Mieville, P., Carnevale, D., Caporini, M. A., Gajan, D., Copéret, C., Lelli, M., Zagdoun, A., Rossini, A. J., Lesage, A., Emsley, L., and Bodenhausen, G.: Dynamic nuclear polarization of quadrupolar nuclei using cross polarization
690 from protons: surface-enhanced aluminium-27 NMR, 48, 1988–1990, https://doi.org/10.1039/c2cc15905h, 2012.

Vogt, F. G., Yin, H., Forcino, R. G., and Wu, L.: ^{17}O Solid-State NMR as a Sensitive Probe of Hydrogen Bonding in Crystalline and Amorphous Solid Forms of Diflunisal, Mol. Pharmaceutics, 10, 3433–3446, https://doi.org/10.1021/mp400275w, 2013.

Zhao, X., Edén, M., and Levitt, M. H.: Recoupling of heteronuclear dipolar interactions in solid-state NMR using symmetry-based pulse sequences, 342, 353–361, https://doi.org/10.1016/S0009-2614(01)00593-0, 2001.

Zhao, X., Hoffbauer, W., Schmedt auf der Günne, J., and Levitt, M. H.: Heteronuclear polarization transfer by symmetry-based recoupling sequences in solid-state NMR, Solid State Nuclear Magnetic Resonance, 26, 57–64, https://doi.org/10.1016/j.ssnmr.2003.11.001, 2004.